CONFERENCE REPORT • OPEN ACCESS

Progress in particular fields of fusion technology presented at the 29th IAEA Fusion Energy Conference 2023

To cite this article: Klaus Hesch 2024 *Nucl. Fusion* **64** 117002

OPEN ACCESS
IOP Publishing | International Atomic Energy Agency
Nuclear Fusion
Nucl. Fusion **64** (2024) 117002 (26pp)
https://doi.org/10.1088/1741-4326/ad7a0c

Progress in particular fields of fusion technology presented at the 29th IAEA Fusion Energy Conference 2023

Klaus Hesch

Karlsruhe Institute of Technology, Karlsruhe, Germany

E-mail: klaus.hesch@kit.edu

Received 17 May 2024, revised 29 July 2024
Accepted for publication 12 September 2024
Published 30 October 2024

Abstract

This paper provides an overview on the progress in fusion technologies presented during the 29th IAEA Fusion Energy Conference held in October 2023 at London, UK, with a focus on the topics ITER technology, heating and current drive technology as well as fusion nuclear technology, including fusion nuclear science as well as technology research devices. A complementary contribution, authored by Amanda Quadling, covers the topics materials development, in-vessel components, licensing & safety, socio-economics and environment, as well as next step machine designs.

Keywords: ITER technology, plasma heating technology, fusion nuclear technology, fusion technology research devices

(Some figures may appear in colour only in the online journal)

1. Introduction

Fusion technology progress reported at the 29th IAEA Fusion Energy Conference 2023 was quite impressive in the areas considered. In particular, the progress and performance in manufacturing of the very large components for ITER, and the lessons learnt, earmark a status of achievement that makes the realization of fusion energy conceivable. Furthermore, a number of important results derived from the JET DT campaigns were presented.

While for ITER technology and also for the heating and current drive systems, the contributions summarized here clearly provide an encompassing view on the state of the art, the overview is certainly less complete in the area of the nuclear technologies, as there were more specialized conferences almost at the same time, drawing a considerable share of the reporting on most recent findings and achievements there. Nevertheless, also in this area impressive progress was shown.

The overview compiled here has been given a more differentiated topical structure than the original attribution. In particular, the contributions are compiled under the headlines 'ITER Large Component Manufacturing', 'ITER Safety Systems and Commissioning Preparation', 'ITER Diagnostics and Plasma Control', 'Microwave Plasma Heating', 'Neutral Beam Plasma Heating', 'Other Plasma Heating Methods', 'Fuel Cycle and Tritium Operation', 'Tritium Breeding Blanket Technologies', 'Fusion Neutron Sources', 'Neutronics' and 'Technology Research Devices', the latter including contributions on JT60-SA, WEST and the Divertor Tokamak Test Facility (DTT).

2. ITER large components manufacturing

The ITER Large Components presented at the conference include the cryostat, the toroidal and poloidal field (TF and PF) coils, the central solenoid (CS) and the correction coils as well as the magnet feeders.

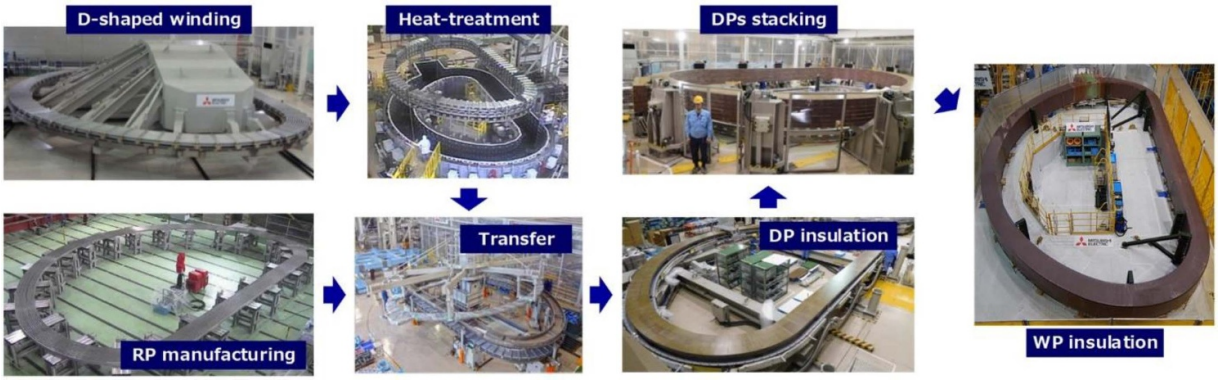

Figure 1. ITER TF winding pack manufacturing steps.—RP: radial plates for mounting the superconductor cables after their D-shaped winding and heat treatment; DP: double pancake, assembly of a radial plate filled with superconductor cables from both sides, including all necessary insulations; WP: winding pack, assembly of 7 double pancakes, to be enclosed by structural components to form a toroidal field coil. Reproduced from [2].

The largest component manufactured for ITER obviously is the ITER cryostat, contributed by ITER India. A report on challenges and lessons learnt was given by Bhardwaj *et al* [1]. Being one of the largest vacuum vessels ever built (∼30 m diameter, ∼30 m height) and classified as Protection Important Component, this element presented numerous challenges that have been successfully mastered up to the installation of the lower two of the in total four parts in the ITER Tokamak Pit. Made of austenitic stainless steel, it has a total weight of more than 3850 tons, while providing support, in the final stage of tokamak assembly, to components with a total weight of more than 21 000 tons. It has to provide vacuum thermal insulation (10^{-4} Pa) for the superconducting magnets operating at 4.5 K and for the thermal shield operating at 80 K. Moreover, it provides ∼300 penetrations for all the systems necessary to operate and maintain the tokamak. Manufacturing was done in four parts, i.e. the Base Section, the Lower Cylinder, the Upper Cylinder and the Top Lid, and at three places, i.e. the Indian factory (sector manufacturing), the ITER site workshop (subassembly for sections) and the Tokamak Pit (installation of sections). To master the challenges of welding of higher thickness weld joints (50–200 mm) with tight tolerances, a number of welding, non-destructive examination and in-situ tracking methods were studied in sector mock-ups to establish the best-suited combination of methods and manufacturing sequences. For the composition of the Base Section in the ITER site workshop, Narrow Gap Hot Wire TIG welding was selected as the preferred method, while ultrasonic testing turned out as best-suited non-destructive testing approach. Bottom line, the resolution of technical challenges at different stages under one unique Cryostat Team with different stakeholders turned out to be a win-win situation for all.

The lessons learned from the development and the production of the ITER TF coils, which was done in parallel in Japan and the EU and successfully concluded in 2023, were presented by Hemmi [2]. This cutting-edge technology, applying Nb_3Sn superconductor cables, has thus been made available for large tokamaks, and can be used as the basis for DEMO machines. Sticking to low-temperature superconductors for cost and maturity reasons in 2007, the required critical current density of 360 A mm^{-2} at a field of 11.8 T imposed the choice of the superconductor. As Nb_3Sn becomes superconducting (and brittle) only after a heat treatment, which induces dimensional changes in a close-to-use geometry ('winding pack'—figure 1), care had to be given to the accurate laser tracking of the change of the superconductor trajectory during this process.

To allow the manufacturing of the final supporting structures, the radial plates, in parallel, accurate prediction of this change was developed and utilized. Also for the electrical insulation in a neutron irradiation environment a new, specialized procedure had to be developed. In result, a combination of a cyanate-ester resin and polyimide-glass-cloth tape was used, in a specific configuration allowing the ester to penetrate and fill all gaps without producing too much heat during reaction/curing. Also this valuable knowledge and experience is now available for huge tokamaks in general. For the welding of the structures encapsulating the superconductor winding packs, both-side welding was employed to reduce welding distortions and thus reduce the need for extra thickness to be machined down to finally achieve the required tight tolerances, saving manufacturing time. The welding deformation control process was described in more detail in a poster by Kajitani *et al* [3]. For the application, the Current Centre Line (CCL) in the magnet windings has to fulfil severe tolerances of a few mm within overall coil dimensions of 16.5 m × 9.2 m. Thus, the CCL had to be marked, and tracked throughout all manufacturing stages, by means of holes drilled into the structure to allow laser tracking. In result, all coils fulfilled the CCL position requirements, and the CCL positioning procedure is now established for huge TF coils. Thus, the manufacturing and delivery of all (18 plus 1 spare) TF coils has been completed in October 2023, 15 years after the manufacturing of the Nb_3Sn strands had started in 2007.

The presentation by Martinez Lopez (on behalf of Bonito Oliva *et al*) on the ITER PF coils [4] was focussed on management and logistics issues only, without addressing new technical issues/technological solutions. It became clear that the management issues discussed (performance of suppliers, procurement management) actually were a consequence of

the route F4E had chosen for the realization of the PF coils, i.e. focus on price and competition of industrial suppliers without in advance securing the necessary technological competence. At the same time, the realization of the PF coils 1 and 6 (PF1 in Russia, PF6 outsourced by F4E to China) did not face such problems, as there, competent big research institutions (Efremov Institute, ASIPP) equipped with the necessary resources were entrusted with the task. So, the actual 'lesson learned' is about the way to realize technologically challenging, first-of-a-kind components, while the procurement and supplier management approaches and principles that had to be adopted are important to note, but not actually new.

In contrast to the above, the report by Wooley *et al* on the experiences made and solutions developed during the manufacturing of the ITER CS [5] is a valuable account on the numerous technical challenges met for this high performance component, which has to survive 30 000 slow discharge cycles in different scenarios—from the qualification of the superconductor cable materials through the different manufacturing and testing steps up to the interaction of the design with transportation mode and precautions. Moreover, it highlights with many technical examples a management approach that builds upon pre-qualification, mock-up and performance testing at each of the many stages, with direct feedback to the preceding steps including the different layers of design. In particular, the production of a mock-up qualification coil with copper instead of superconductor strands, and 16 instead of 40 14-turn layers of one CS segment, had turned out to be extremely helpful for validating the manufacturing design of the coil and improving the validation of the tools and processes before utilizing superconductor. Another highly valuable experience was the optimization of the coax joints connecting the CS modules to the electrical feeders. Here, tests done both at General Atomics and at the SULTAN test facility in Switzerland led to the identification of a weak point in the joint sequence, and to a way to remove it. Moreover, testing of each of the six plus one spare CS modules under conditions similar to the ITER operational environment led to the identification of opportunities for improvement during testing of each of the three first modules that were implemented subsequently. A particularly important result is the full paschenization of components at module voltage.

The presentation by Lu *et al* on the lessons learned from the Correction Coil and Magnet Feeder realization [6] provided relevant insights on pipe welding techniques for superconductor cables as well as on the importance of, and working solutions for, Paschen-tight insulation of cables, connectors and feedthroughs even under challenging spatial conditions.

3. ITER safety systems and commissioning preparation

Here, a focus was on the ITER Disruption Mitigation System (DMS)/Shattered Pellet Injection System (SPI—figure 2). M. Lehnen gave an overview talk addressing both the status of technical developments and of the modelling/simulation/validation work within the international ITER Disruption Mitigation Task Force, involving 23 institutions through collaboration agreements and contracts [7]. This first-of-a-kind system, designated to protect ITER components from excessive heat and electromagnetic loads including runaway electron effects passed its preliminary design review in 2022. Technical solutions for pellet formation (in different compositions), pellet acceleration, gas shielding, shattering and optical control as well as pellet synchronization for multiple injections have reached a high level of maturity, where many parameters of the ITER baseline (e.g. pellet dimensions, speed) have already been met. Modelling efforts employing the codes DREAM, INDEX, JOREK, M3D-C1 and NIMROD and validation experiments at JET, DIII-D, K-STAR and ASDEX Upgrade have provided a good level of understanding of the effects of pellet composition, multiple injections and the time intervals in between, while optimization of injection scenarios still remains a challenge.

This presentation was complemented by two posters by Gebhart *et al* [8] and Zoletnik *et al* [9], both addressing the 'firing' process of large (28.5 mm diameter) hydrogen pellets in order to ensure pellet integrity before shattering. This turned out to be a challenge as such pellets have not been used on present-day devices, and internal strength is not very high. Another challenge is in limiting the amount of propelling gas arriving to the plasma before the pellet, as this could both exceed the specified limits for explosive gas inventories of the port cell and trigger early disruption. Gebhart *et al* provided an account on the meticulous efforts at ORNL, making use of the ORNL SPI test bed, to understand and optimize the firing process and pellet speed, and to reduce the amount of propellant gas required. As a result of studying different valve types and breech geometries, and developing models for the propellant gas flow, forces on the pellet, and reaction of the valve/breech on the electric signal, an optimum case could be determined for the given parameter space. There is a valuable modelling tool box now, that will be used to inform and further optimize the ITER SPI design. In parallel, a high-pressure propellant valve also has been developed at the DMS support laboratory at CERES, Budapest, where the production, launch and shattering of large pellets have been have demonstrated, too, as reported by Zoletnik *et al*. The effect of the gas flow during de-sublimation on pellet integrity during firing was established and various automated pellet recipes were developed by time dependent control of the gas feed rate, barrel pressure and cold head temperature. A novel, radiation compatible Optical Pellet Diagnostic concept has been developed and demonstrated which could be used as part of the real-time control of the DMS system.

Different from the SPI for disruption mitigation, continuous pellet injection for core fuelling is required, too. Baylor *et al* [10] presented quite relevant ORNL work on comparing and optimizing two different, continuously working extruding systems for DT fuel, demonstrating reliable pellet size and speed control for many minutes of operation, which in principle can be extended to continuous operation, and

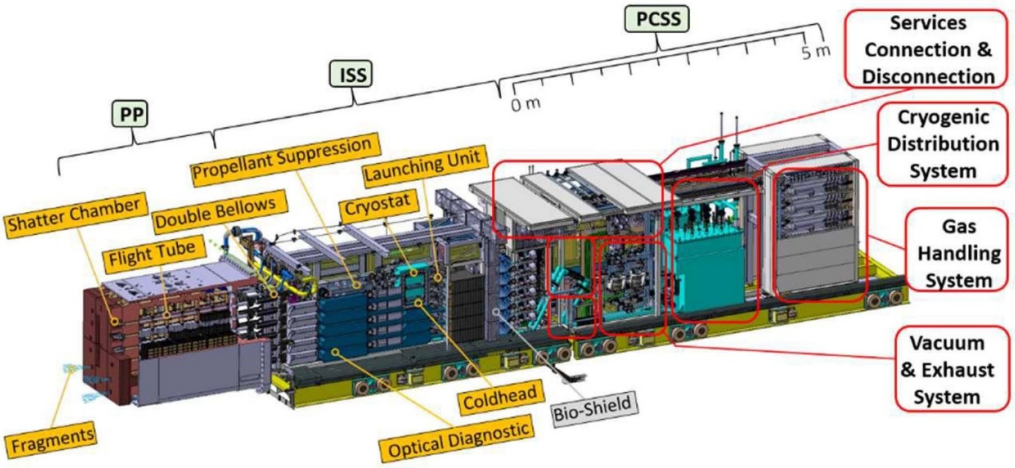

Figure 2. Present ITER Disruption Mitigation System design in equatorial port plug #2. Reproduced with permission from [7].

addressing recirculation both of excess extruded materials and of propellant gas.

Important work towards another highly relevant ITER safety system, the Vacuum Vessel Pressure Suppression System, was presented in a poster by Aquaro *et al* [11]. Experiments were done with a large-scale set-up at the University of Pisa, studying steam sub-cooling in a water reservoir, at ITER-relevant conditions different from anything that could be derived from nuclear fission facilities. Conditions for avoiding Condensation Induced Water Hammer and 'chugging', i.e. bubble formation, by the addition of non-condensable gases were determined.

In the case of a loss-of flow accident in the ITER divertor, temperature will rise during continued plasma operation, and even more during the subsequent disruption initiated by the Fast Plasma Shutdown System. This can lead to melting, destruction of divertor components, and even water ingress into the tokamak. El-Morshedy [12] could demonstrate in a modelling approach using the previously developed ITERTHA code, that swirl inserts in the cooling tubes in general help to keep the temperatures lower in critical parts of the component. Irrespective of the absolute temperature values, which of course depend on the assumptions made, this could be an important advantage in an accidental case.

The lessons learned from JT-60SA commissioning, including the consequences from the arc incident on one of the superconducting magnets in 2021, that will be quite valuable for the commissioning of ITER and subsequent fusion devices, where shown by Shibama *et al* [13]. Particularly the introduction of local vacuum testing of critical barriers prior to the overall pump-down, and of a high-speed vacuum interlock system based upon a cold-cathode gauge and rapid shut-down of the superconducting coil power supplies appear to be highly relevant. Arcing under Paschen conditions was the topic of Roy *et al* from IPR India, too [14]. Here, experiments were presented for testing electrical insulation vacuum barriers of different compositions in a configuration simulating the situation at the PF coil connector of the tokamak SST-1, and related simulations of the electrical field around.

The concept of the ITER blanket remote maintenance system inspired a team at the University of York to an approach for developing a workflow for an automated maintenance system for future power plants, shown by Devlin-Hill *et al* [15]. The aim is to handle within the minimum time possible the consequences of vertical displacement events (VDEs) of the plasma, which can cause severe damage to the First Wall, integrating the JOREK-STARWALL plasma simulation code for predicting the damage with machine learning techniques for instructing the automated remote maintenance system.

4. ITER diagnostics and plasma control

A considerable amount of progress was presented in the area of ITER diagnostics and plasma control, with focus on visible and infrared diagnostics, Diagnostic Neutral Beams (DNBs), neutral particle analysis, Thomson Scattering, neutron and nuclear analysis and magnet control systems.

The ITER infrared and visible wide angle viewing system is a critical element for machine protection, physics analysis and plasma control. The optical and mechanical port design of the Equatorial Port 12, one of the five ITER ports hosting this system and a ´first plasmà component prototypical to other systems, has been brought to maturity for the final design review. The design status, including electromagnetic, thermo-mechanical and nuclear analysis and prototypical validation by the realization of critical components, i.e. pneumatic shutters, mirrors, lateral walls and flanges, developed in a collaboration of CEA, CIEMAT, Bertin Technologies, INTA and F4E, was presented by Vives *et al* [16]. Complementary, the advances by a joint team from CEA/WEST, UKAEA, and the universities of Paris-Saclay, Aix-Marseille and Basel on improving the accuracy and reliability of the IR diagnostics for ITER were presented by Aumeunier *et al* [17]: the IR measurements for temperature imaging are compromised by changes of reflectivity of metal surfaces and multiple reflections. By introducing a new numerical approach including 'forward' simulation of expected IR images in different plasma situations and machine

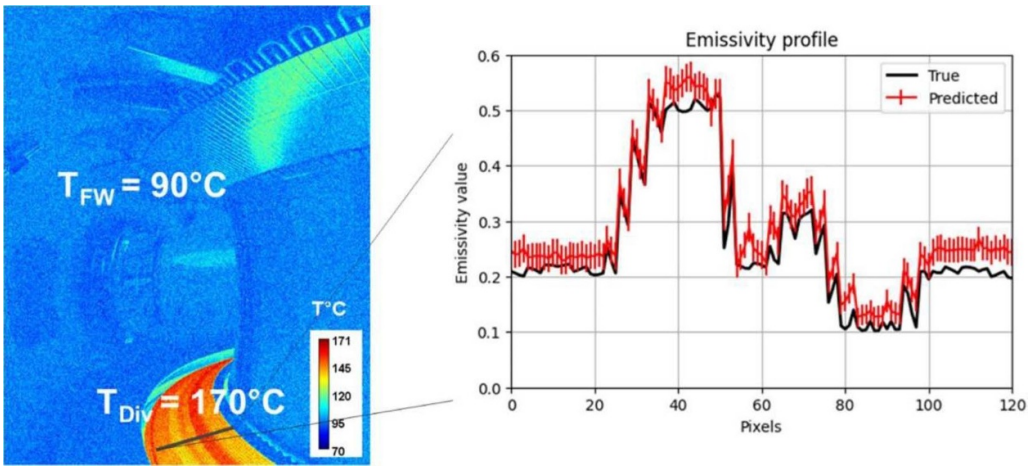

Figure 3. Left: simulated image of wide-angle tangential view in the case of divertor baking at 170 °C and wall baking at 90 °C. Right: true and predicted emissivity profile on WEST lower divertor from convolutional neural network trained from synthetic database. The simulated test images are noised to account for measurement uncertainties, which causes predictions uncertainties shown as error bars. Reproduced from [17].

learning making use of neural network methods, the accuracy of the temperature imaging could be enhanced to become better than 10% as demonstrated on WEST (figure 3—see also [18]). Furthermore, ELM situations have been included in the database.

The ITER DNB System will allow estimating the He ash content in the plasma by charge exchange recombination spectroscopy. It is being developed at IPR India, and the progress on several lines of development was shown. This includes the lessons learned from the development of beamline components, i.e. the Neutralizer made of CuOF and the Residual Ion Dump made of CuCrZr, that were presented by Joshi *et al* [19]. Difficulties, i.e. cracks due to residual stress, had occurred with deep dissimilar e-beam welding for cooling water connections. Thus, the process was replaced by shrink-fitting followed by electro-deposition. For high voltage resistance of the Residual Ion Dump, which has panels at −8 kV as well as at ground potential, the positioning of some bolts in the original configuration had been found unfavourable, i.e., leading to unexpected arcing, possibly due to stress in the insulation layer. Therefore, an improved geometry was introduced, ensuring a sufficient gap between ground and HV potential bolts. The design of the Drift Duct, consisting of two concentric bellows connecting the DNB vacuum vessel and the tokamak, has been validated through a series of load cases according to RCCMR and EN14917 codes down to the level of subcomponents, weld-zones and bolts, as reported by Muvvala *et al* [20]. The relevance is in the fact that the Drift Duct is a Protection Important Component w.r.t. vacuum and radioinventory containment, which has to mechanically decouple the tokamak from the DNB vessel in all cases (e.g. large displacement in axial and lateral movement, pressures and temperatures. The design study for the stainless steel vacuum vessel that will contain the entire DNB system, and will constitute part of the ITER first confinement barrier for vacuum and tritium thus being a Safety-Important Class 1 component, was presented by Yadav *et al* [21]. Particular challenges are in the vacuum sealing of the top lid of the 68 t, $9.6 \times 5.7 \times 4\ m^3$ component, which will be removable for maintenance access. The double metal sealing has a rectangular shape like the entire DNB box and a total circumference of 25 m, and thus constitutes, according to the authors, the largest-ever configured one. Simulation of sealing compression load homogeneity, as well as of welding efficiencies and weld stress distributions of the vessel elements in order to determine post-weld machining needs and to secure deflections within specifications were done. W.r.t. to the realization of the Indian Test Facility for the ITER DNB system, D.K. Sharma presented the entirely indigenous development and realization of the high-voltage bushing, providing vacuum-tight 100 kV insulation for all the supply line feedthroughs to be connected to the negative ion source at this potential, against the vacuum vessel at ground potential [22]. Connecting all the different lines in the proper way to the 800 mm diameter, 530 mm long porcelain cylinder as the shape-defining element of the bushing, posed a number of design & manufacturing challenges, which all were tackled and resolved.

Different from smaller tokamaks, the functions of plasma current control, plasma shape control, and vertical stabilization will be combined in the ITER Plasma Control System, because of a higher level of coupling between control circuits, the long time required for control fields penetration into the plasma and actuator sharing for different control purposes. An axisymmetric magnetic control architecture taking this into account has been elaborated by Consortio CREATE together with ITER, and presented by Mattei *et al* [23]. The control architecture has been tested with simulations of a ramp-up segment including X-point formation using a voltage control scheme and of a flat-top plasma with a VDE, showing satisfactory performance so far. Another interesting approach, also presented by Mattei *et al*, by CREATE, Napoli University and ITER [24] addresses a semi-automated start-up procedure for large tokamaks, taking into account currents induced in the structures and other constraints like limitations on

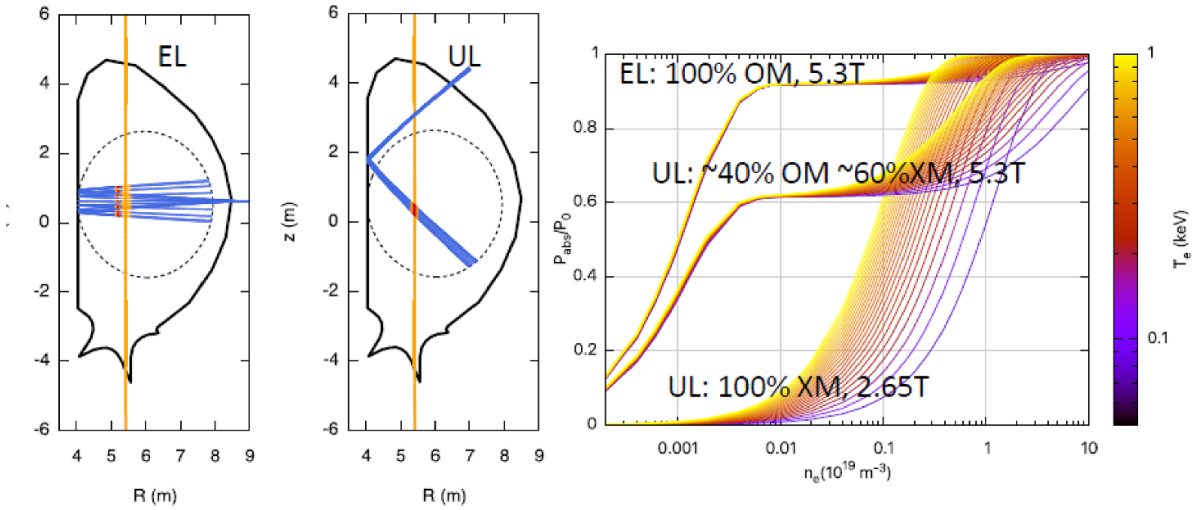

Figure 4. EC power absorption in ITER. Upper launcher (UL) and equatorial launcher (EL) cases for different frequencies and toroidal fields. Reproduced with permission from [24].

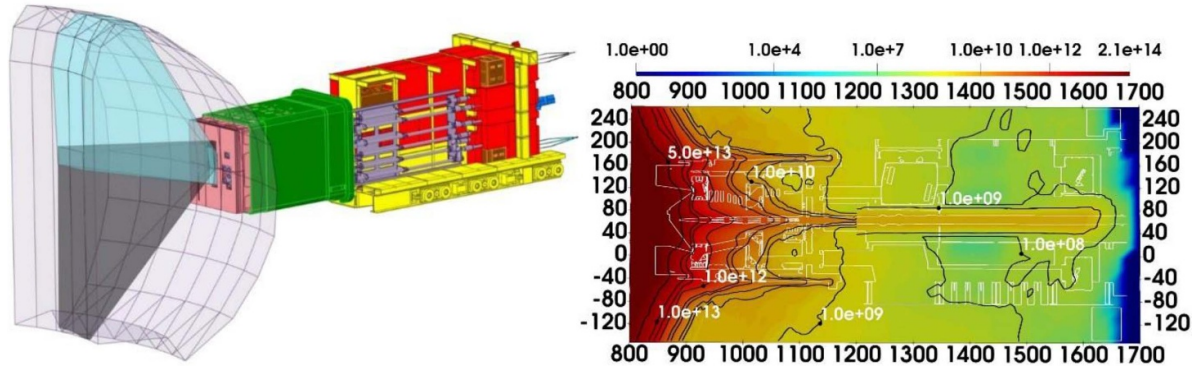

Figure 5. ITER equatorial port 11, model 2022 (left) and neutron flux map (right). Reproduced with permission from [25].

active control coil circuit voltages, as well as EC heating. The approach combines the CREATE-beam dump (BD) code for optimizing active circuit currents, BKD0 for predicting the evolution of the main plasma parameters, and the quasi-optical beam tracing code GRAY for EC power absorption, and was applied for two case studies with JT-60SA and ITER parameters (figure 4). As the integrated code can be run in short times (<1 min), it is suggested to use it for intra-shot optimization.

Portnov, Mukhin and Shevelev provided progress reports on the work done at, or coordinated by, the Joffe Institute towards ITER diagnostics. The poster presented by Portnov *et al* [25] summarized improvements implemented in the ITER diagnostic ports UP8, EP11 and EP8 on the basis of advanced neutronics analysis (figure 5). Mukhin´s *et al* poster addressed the ITER Divertor Thomson Scattering diagnostic system [26], focussing on improvements in reliability and lifetime of the lasers towards longer maintenance intervals, of safety aspects of the laser input windows, polychromators and the collecting optics, particularly, the plasma-cleaning of the first collecting mirror. The poster by Shevelev *et al* [27] illustrated the progress made towards the design of the ITER Neutral Particle Analyzer (NPA), i.e. reaching the stage of final design preparation. It highlighted two systems to be located in the NPA neutron dump, the Neutron Spectrometer and the Gamma-Ray Spectrometer, increasing the range of detected radiation fluxes by making use of various gamma-ray and neutron detectors in combination with neutron attenuators. The entire system is designed to measure the fluxes and distribution of uncharged fusion products outside the vacuum chamber and may thus be of interest for other new generation facilities, too.

Fibre-Optical Current Sensor (FOCS) measurement foreseen for plasma current control in ITER relies on the change of polarization angle of linearly polarized light travelling through an optical fibre, caused by the longitudinal magnetic field in the fibre induced by the current. To establish the effect of 14 MeV neutrons on the measurement method, JET TT and DT campaigns were used. In result, as reported by Gusarov [28], it was derived from parallel measurements with Rogowski coils and neutron detection that the FOCS measurements remained un-effected by the neutron flux. However, it was found that a fibre-optical sensor which had been exposed to temperatures of 200 °C–300 °C, well above the specified operation temperature range up to 85 °C, had degraded, likely because a deterioration of the fibre polarisation properties.

For the remote operation of future fusion facilities, Schissel *et al* proposed the remote operation system developed at DIII-D and stress-tested during the Covid-19 pandemic as a basis [29]. It includes secure methodologies to allow remote control of hardware including the plasma control system application, as well as secure methods to enable the on-site team to closely coordinate their work with remote team members. W.r.t. ITER operation, the set-up of an ITER computational grid and an ITER Remote Experimentation Center is proposed, in order to substantially increase the computational power available to the ITER project, and to enhance near-real-time data analysis to inform control room decision making by involving a wide group of experts worldwide.

5. Microwave plasma heating

A. Bruschi provided an encompassing description of the status of the conceptual design development towards the EU DEMO Electron Cyclotron Heating (ECH) system [30]. A modular approach has been chosen, making use of clusters of gyrotrons and transmission line components, to ensure flexibility w.r.t. evolving design parameters for the tokamak and the plasma. Flexibility is also implemented by designing the gyrotron tubes and the EC system for accommodating four microwave frequencies ranging from 136 GHz up to 238 GHz for different EC-wave applications, such as plasma start-up assist, bulk heating, as well as control of Neoclassical Tearing Modes (NTMs) and radiative instabilities. If frequency tuning in a narrower range proves feasible for the sources and the optics, movable mirrors close to the plasma for NTM stabilization can be avoided. The overview addresses all main components of the system, i.e. the gyrotrons as the microwave sources, the transmission lines (figure 6) with their different elements, and the antennas/launchers facing the plasma, with a particular focus on the arrangement of the different transmission line elements in a spatially restricted environment. Targeting a total power of 130 MW, sufficient to provide all necessary heating power for the 'ECH-only' approach, the system will be based on 2 MW coaxial cavity gyrotrons which should reach a level of 98% individual reliability, in order to secure highest-possible system reliability. The power will be needed not only for bulk heating (30 MW), but also for counteracting NTM instabilities (30 MW) and radiative (edge) instabilities (70 MW) that may be expected from the W First Wall influence.

The conceptual design of the STEP heating and current drive system, that will be based exclusively on microwave sources providing either electron cyclotron (EC) or electron Bernstein wave (EBW) coupling, was addressed by Henderson *et al* [31] and Freethy *et al* [32]. Efficiency (w.r.t. cost of electricity), modularity and flexibility as design drivers in a compact spherical tokamak machine, that is conceived to be fully non-inductive (with 80%–90% bootstrap current), had been translated into 10 selection criteria like current drive and electrical efficiency, plasma start-up and ramp-down capability, current profile control, impact on other tokamak systems and on cost as well as technology maturity and reliability, availability, maintainability, inspectability. These were applied to a wide range of plasma heating systems, resulting in the EC/EBW selection, with a total power up to 336 MW (170 MW EC and 120 MW EBW, with a certain top-up to compensate for plasma variations). Multiple scenarios are being investigated using either EC or EC and EBW, with power requirements ranging from 50 to 170 MW. In fully non-inductive steady state operation, the required current drive across the plasma cross section can, according to the simulations, be achieved with a net electric power of only ∼100 MW, while the ramp-up and stabilization may require, in short phases, the full power capacity installed. In parallel, UKAEA is developing a 1.8 MW EBW system for MAST-U to validate the current drive capabilities of EBW. The key parameters, the system layout and the status of each of the major subsystems were shown by Webster [33]. The system, relying on two dual-frequency gyrotrons operating at 28 and 34.8 GHz, will provide 1.8 MW (1.5–1.6 MW to the plasma) via two steerable launchers (on-axis and off-axis).

Marsen *et al* [34] highlighted the improvements implemented in the ECRH system of W7-X after the earlier operation phase OP1.2, and tested since 2022 in the operation phase 2.1, as well as further planned measures, in order to increase the reliability and average available power. Installing air dryers in the beam ducts, faster arc detection and protection from overcurrent in the gyrotron body circuit yielded an increase of pulses without interlock from 84% to 92%. From the experience so far, further work will be dedicated to implement the possibility in the control system to quickly re-start a gyrotron after tripping, in order not to loose the power for the rest of the pulse. The high-density high-performance discharges of W7-X operate in the O2 mode, where adapted polarizing mirrors at the torus walls provide optimum multibeam transmission through the plasma to counteract the lower O2-beam absorption.

Significant progress in gyrotron development in Japan was reported by Ikeda *et al* [35] und Kariya *et al* [36]. The QST team achieved an outstanding result i.e. 1 MW output for 30 s both at 170 and 137 GHz, and 0,9 MW at 104 MHz, with a triple-frequency gyrotron developed for ITER (figure 7), and introduced new heater power control schemes to ensure flexible and stable gyrotron operation. New encouraging experimental results were also shown by the team around NIFS and Tsukuba university, i.e. up to 1 s operation of a 154/116 GHz dual frequency gyrotron developed for LHD, and first short pulse results of the Cannon 28 GHz gyrotron with depressed collector operation and good efficiencies. The Cannon 28 GHz gyrotrons are employed on the magnetic mirror device Gamma10 and the steady-state spherical tokamak QUEST in Japan. While up to now, these gyrotrons had been equipped with a single CVD diamond window, a double-disk sapphire window with fluor-carbon face cooling was successfully applied. ITER India has now successfully commissioned a cw-MW class gyrotron test facility with all necessary auxiliary systems using a purchased 170 GHz, 1 MW gyrotron as reported by Rao *et al* [37].

The status of the ITER equatorial ECH launcher design under development at QST was shown by Kajiwara *et al* [38].

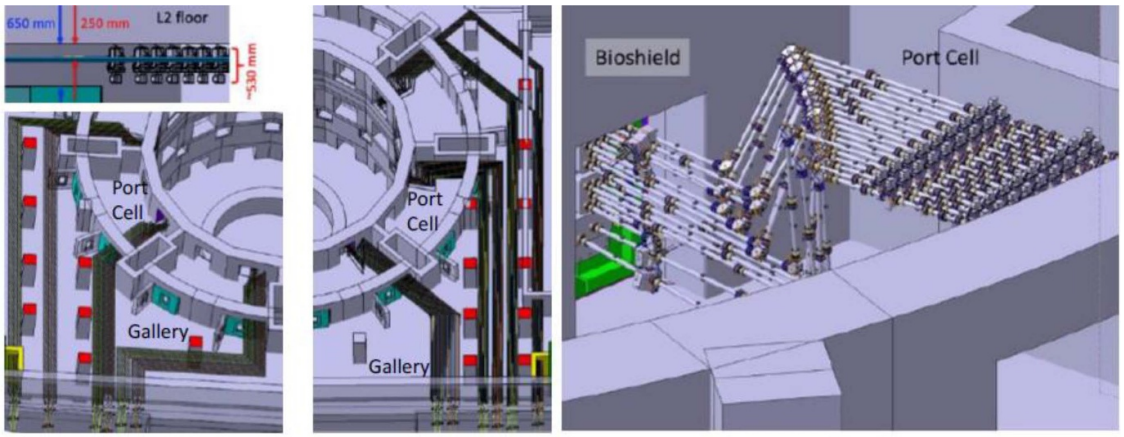

Figure 6. ECH transmission lines for EU DEMO. Top left: side view of the lines running close to the ceiling of the equatorial level. Bottom left: evacuated waveguides (EWGs) routing to ports 8, 10 and 12. Centre: EWG routing to ports 14, 16 and 2. Right: EWG routing and components in the port cell. Reproduced from [30].

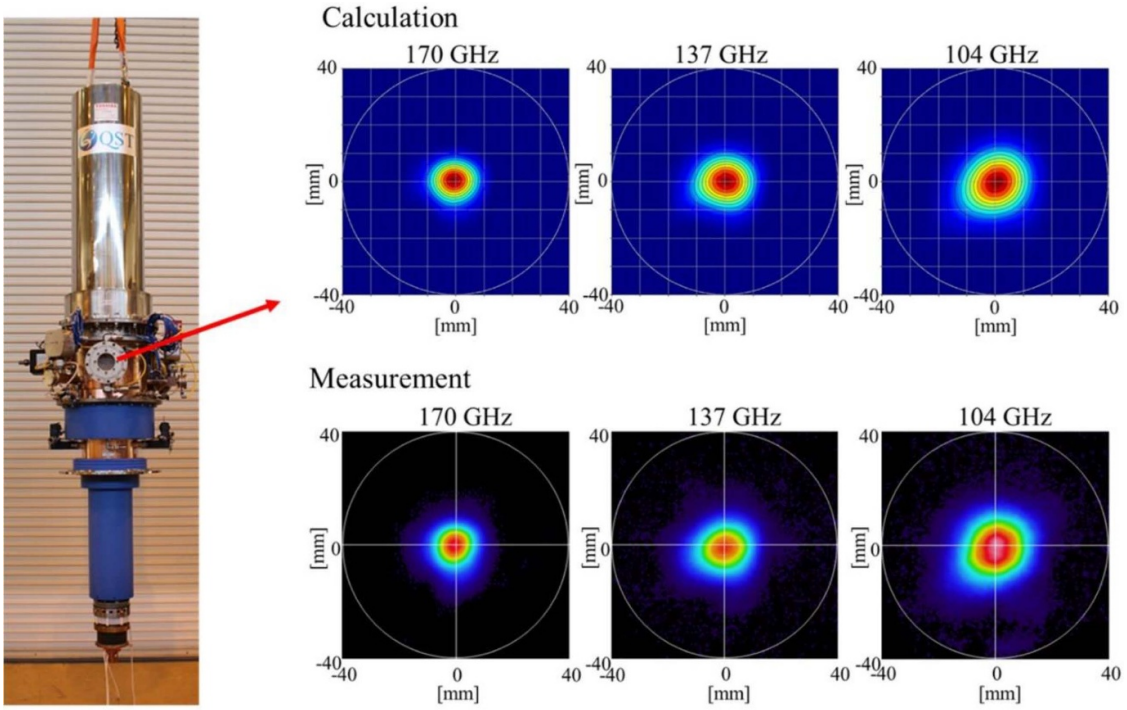

Figure 7. *(a)* Photo of triple-frequency gyrotron; *(b)* calculation and measurement of RF-beam-patterns at 170 GHz, 137 GHz and 104 GHz on the gyrotron output-window-flange. Reproduced with permission from [35].

Following an ITER project change request in 2020, the entire optical design of the launcher had to be changed in order to widen the hands-on maintenance access channel from 50 to 90 cm with a view to the use of human radiation protection equipment. Up to now, the design change as well as mock-up validation of optical components and of the full-scale prototype assembly of the moveable front steering mirror (w.r.t. angle scan speed) have been achieved, and the Final Design Review is foreseen for the beginning of 2025. For the ECH system of JT-60SA, the performance of a large diameter, triple-frequency corrugated waveguide has been validated in the integrated commissioning phase, as reported by Yamazaki *et al* [39]. On the basis of the good agreement between the calculated values, assuming 1 mrad tilt angle at each of the 15 mitre-bends, and the measured transmission efficiencies of 80/82/85% at 82/110/138 GHz, the transmission line design for the JT-60SA initial experimental phase has been completed.

A new approach by General Atomics to dielectric-lined waveguides for EC radiation of particularly high frequencies for high power, high-field EC Heating or wide frequency ranges for EC Emission diagnostics was presented by Thackston *et al* [40]. This refers to the limitations w.r.t. machining of quarter-wavelength corrugations for frequencies

at or above 300 GHz and the frequency-dependence loss mitigation at fixed corrugation periods. Modelling suggests clearly improved attenuation in both cases; experimental evidence however could not yet be provided in the reported power handling studies due to a mismatch of the waveguide dimensions and the available high-power gyrotron frequency.

6. Neutral beam plasma heating

In the recent JET DT experiments with world record fusion energy output, the D and T neutral beams did play an important role not only for plasma heating, but also for fuel provision. To enable accurate interpretation of the fusion energy and plasma parameter measurements, accurate calibration of the T neutral beam injection is essential. As there were doubts about this, a new calibration method was developed, and presented by King *et al* [41], analysing transients of stored energy in dependence of D and T beams and making use of the well-established calibration for the D beams. In result, T beam calibration could be brought an accuracy of 10%, comparable to that for the D beams.

The preparation of the ITER neutral beam heating system relies on a step-ladder approach, involving, inter alia, the neutral beam test facilities at IPP Garching and the full-scale ITER Neutral Beam Test Facility (NBTF) at Padova, Italy in a collaboration involving several ITER partners. The latter had to face quite a number of difficulties in the completion and beginning operation phase. An overview on the recovery measures already implemented or planned was given by Toigo *et al* [42]. For the one-to-one copy of the ITER neutral beam ion source SPIDER, improvements on RF circuits, plasma box, accelerator grids and diagnosability have been implemented during a shut-down phase and are to be checked for effectiveness when operation will be resumed (figure 8).

Ichikawa *et al* [44] reported on efforts to recover the power-supplies of the full-scale prototype of the entire ITER neutral beam injector, MITICA, after a breakdown in so far non-identified positions in the high-voltage plant. In particular, the examination of the electrical behaviour of the power supply system by impulse testing with lower voltages led to the design and implementation of a new monitoring system localizing potential breakdowns, and of a new electrical reactor/resistor/capacitor protection system. Furthermore, a number of components (failed elements of the power supply, RF oscillators) will be replaced and additional protections installed before integrated commissioning. The overall time schedule is under revision. The recent input provided by the IPP test systems, BATMAN Upgrade and ELISE, to both ITER NBI and the NBTF, were highlighted by Fantz *et al* [45] (figure 9).

ELISE succeeded in validating the ion source performance for hydrogen in a sequence of 1000 s pulses, while deuterium turned out to be more difficult because of an increase in the co-extracted electron current. Here, an actuator in the form of biasing the control plate around the plasma-facing grid of the ion source was identified. Ichikawa *et al* [44] also reported on the examination of the mechanical structure of the 1 MV transmission line at the NBTF w.r.t. seismic resistance and radiation protection if applied at ITER and penetrating the tokamak building as tritium safety barrier. In result, the mechanical design was found unsatisfactory for the ITER conditions, and a new, displacement-absorbing structure with special, 6 m long bellows was designed.

The beam divergences of 10–15 mrad so far obtained from different RF driven negative ion sources are significantly above the ITER requirements of 7 mrad, postulated w.r.t. transmission efficiency. Spatially resolved beam power density measurements and modelling attempts were made at BATMAN Upgrade to understand the reasons and reported by den Harder *et al* [46]. So far, the matter is not yet fully understood, but the beam-perpendicular ion temperature, increasing with decreasing source filling pressure, seems to play a role. The same issue is being addressed now at NIFS in a cooperation with IPP, by combining a filament-driven arc negative ion source, yielding typical divergence values between 5 and 8 mrad, with an RF driven source in a hybrid arrangement as reported by Nakano *et al* [47]. So far, first discharges have been successfully demonstrated. From extended modelling at BATMAN Upgrade [46] it was concluded that at nominal power conditions, the ITER transmission requirements though can be satisfied up to a perpendicular ion temperature of $\sim$9 eV, while the values observed so far are in the 2–4 eV range.

Another experimental set-up in support of ITER NBI is the MeV Test Facility at QST. Here, acceleration of a H^- beam up to the ITER specifications for the initial operation phase of 870 keV ion energy, at 230 A m^{-2} for 300 s is targeted. To arrive there, several measures have been successfully implemented as reported by Tobari *et al* [48]. These include a protection system for the filament of the arc-driven negative ion source (different from the RF driven ion source envisaged for ITER) to prevent critical damage, active cooling of the plasma grid to stay within the optimum temperature range for surface ion production, and real-time monitoring of the ion beam divergence angle for feedback control and beam optimization of beam source operation. Bottom-line, beams of 275 keV ion energy for 300 s, and of 745 keV for 10 s, have been achieved so far.

A different aspect of ITER NBI is neutron and photon penetration through the beam ducts to the outside. Simulations applying MCNP6 and GEANT4 to different potential shielding materials were shown by Osei-Mensah *et al* [49], generally pointing to a high shielding effectiveness for 304B7 stainless steel, followed by Ni base alloys, and to a relatively good agreement between the MCNP6 and GEANT4 results. Simulation studies applying the geometry of the ROBIN negative ion source at IPR India were presented by Shah *et al* [50]. Preliminary results indicate that the walls have a distinct impact in terms of potential drops and variations in the structure of the plasma in the plasma grid, i.e. the exit region, leading to splits in ion velocities and in density gradients and diamagnetic drifts, which could explain observed asymmetries in the ion source plasma profile. An experimental study of the influence of permanent magnetic filters, applied in the region

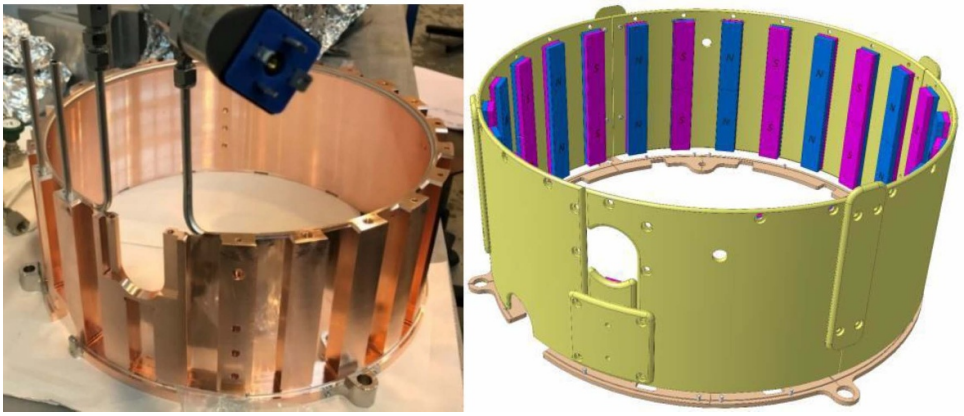

Figure 8. Left: new design of the electromagnetic shield for SPIDER. Right: CAD view of permanent magnets and magnetostatic shield. Reproduced from [43]. CC BY 4.0.

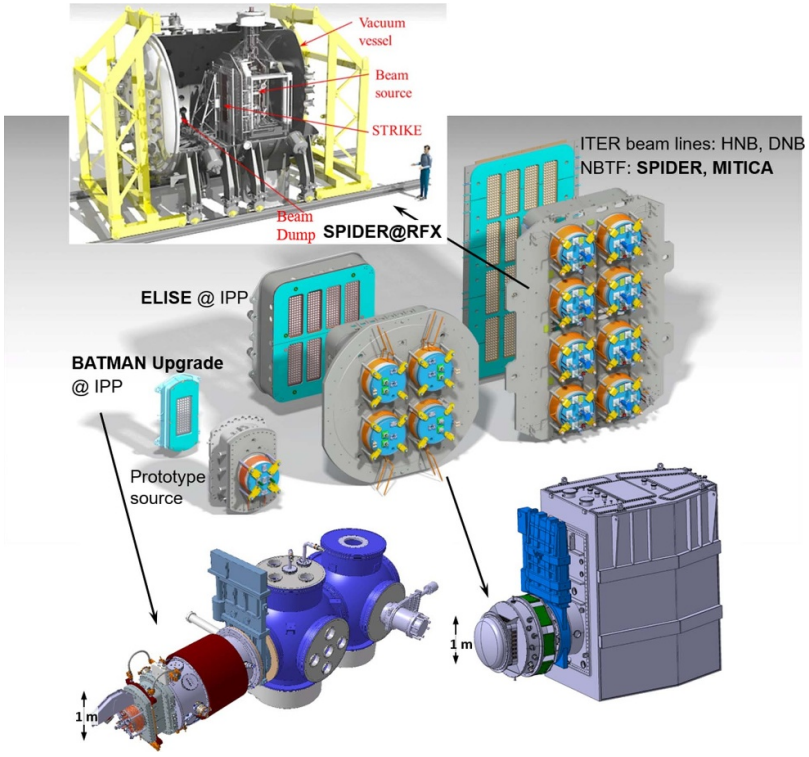

Figure 9. Step ladder approach of the ion source scaling showing the modular ion source, the arrangement of the beamlet groups and the corresponding test facilities: BATMAN Upgrade (BUG) with the prototype source, ELISE with the 1/2 size ion source and SPIDER at Consorzio RFX with the full size ion source used for MITICA and the ITER HNB and DNB. Reproduced from [45]. © 2024 The Author(s). Published by IOP Publishing Ltd on behalf of the IAEA CC BY 4.0.

of the ROBIN plasma grid in order to control co-extracted electrons and filter away high-energy electrons, was presented by Pandya *et al* [51]. In result, fixed magnet arrangements were not found to significantly improve the source performance in terms of electron to ion ratio, while additional tuneable magnetic arrangements near the filter field could be an effective tool to control the co-extracted electrons.

Different from what is planned for ITER NBI, ASDEX Upgrade is operated with positive ion based NBI. Here, a significant improvement had been introduced recently, and the first practical results were reported by Hopf *et al* [52]. I.e. it was demonstrated with one of the ion sources that, keeping the beam divergence at its minimum, the beam power could be decoupled from the particle energy by varying the distance between the extraction grid at the ion source and the acceleration grid (figure 10). Thus, it becomes possible, e.g. to provide more heating power at lower beam energy avoiding shine-through effects at low density discharges, or to tailor the ion-to-electron heating ratio, torque deposition, current drive radial profile as well as the spatial heating power profile. The

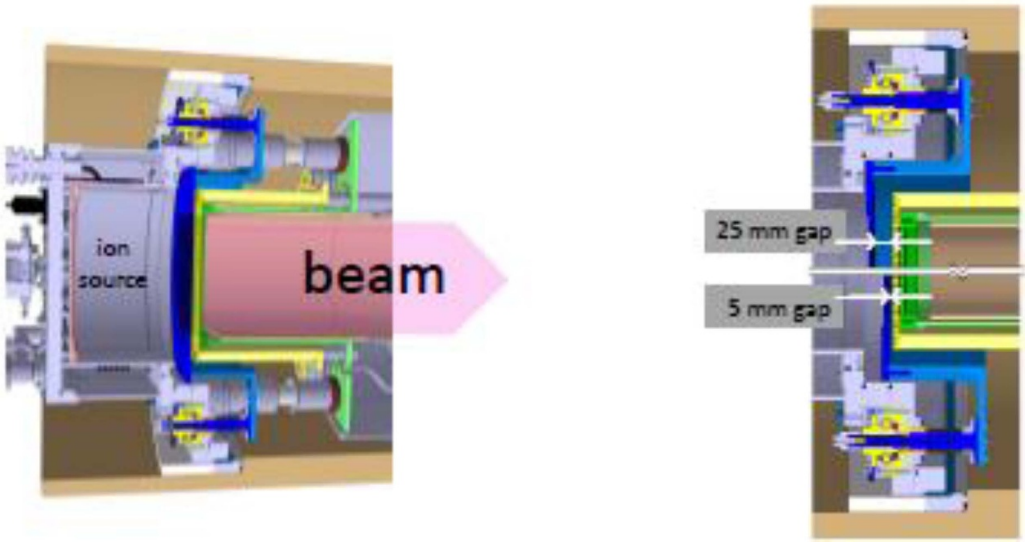

Figure 10. Engineering design of the variable gap: The left CAD rendering shows the ion source on the left, followed by three accelerator grids, the plasma grid (blue, at V_{ex}), the decel grid (yellow, at ≈ -1.5 keV) and the grounded grid (green), at ground potential $V_{gnd} = 0$ V. Source and grids are situated inside the cylindrical main insulator (brown). The extraction/acceleration gap is varied by moving the plasma grid. On the right side, the plasma grid is shown in its two extreme positions. Reproduced from [45].

variable gap effect however would be much lower in negative ion NBI because of the multiple acceleration steps required there.

A bi-directional coupler for 180 kW, 1 MHz radio frequency (RF) input into the 'Two RF driver based negative ion source' (TWIN source) at IPR India was realized and characterized by simulations and low-power tests as reported by Jha *et al* [53]. Insertion losses of −0.01 dB and −43 dB could be measured for the input and output direction, respectively, with a directivity better than −30 dB.

7. Other plasma heating methods

Jacquet *et al* [54] summarized the experience gained from the ion cyclotron resonance heating (ICRH) operation during the JET tritium and deuterium–tritium campaigns in 2021 and 2022. Overall safety requirements included the careful inspection, monitoring and recovery of leak-tightness of the relevant components, in particular, transmission lines and valves, and connection of the venting system to the Active Gas Handling System for potential de-tritiation. For the operation itself, dedicated procedures and system checks were elaborated and successfully implemented to secure maximum performance of the system before starting the tritium pulses, as well as a new control software to optimize voltage distribution among transmission lines to avoid arcing by all means. A concern about 2nd harmonic tritium resonance close to the inner wall could be lifted by demonstrating that no wall heating did occur (figure 11). From the failures and water leaks occurring at the ITER-like antenna, which finally prevented this antenna to be used for the campaign, it can be concluded that fusion reactors should avoid in-vessel integration of complex assemblies, like, e.g. cooling of movable parts or hydraulic actuation. Furthermore, sophisticated procedures were developed to enable the use of ion cyclotron (IC) wall cleaning, with a deuterium plasma and special protections against arcing while 'wetting' the wall with the plasma. W.r.t. the ITER ICRF system, Helou *et al* summarized the status of development in a wide international collaboration [55], at a stage where the ITER re-baselining reduced the number of ports and antennas available for ICRF from two to one. Most relevant aspects are the progress in increasing ICRF coupling while simultaneously minimizing ICRF-specific sputtering, as could be demonstrated on ASDEX Upgrade with high power ICRF operation in a high-Z environment (i.e. tungsten wall), as well as modelling confirmation that 20 MW of power could be coupled into the plasma with a single ICRF antenna as now required for ITER, with modelling tools previously validated on ASDEX Upgrade and JET.

With a view to current-drive requirements in steady-state tokamaks, a new approach for launching lower hybrid (LH) waves from the high-field side into the plasma has been developed at DIII-D and was presented by Wukitch *et al* [56]. In particular, an appropriate launcher for 4.6 GHz LH waves was developed, inter alia with the goal to achieve a driven current density of 40 MA m^{-2}. High-field side launching is expected to be more efficient w.r.t. coupling because of a quiescent scrape-off layer, and better access to the coupling region, as well as being more benign w.r.t. the lifetime of the plasma facing components (PFCs). Here, a new copper alloy with favourable mechanical, thermal and electrical properties was used with the Laser Powder Bed Fusion process, enabling manufacturing of imbedded RF elements and precise waveguide twists and bends. However, the plasma facing materials are required to be either carbon or molybdenum in this approach, materials that so far have been avoided in fusion power reactor concepts. After a test assembly with a

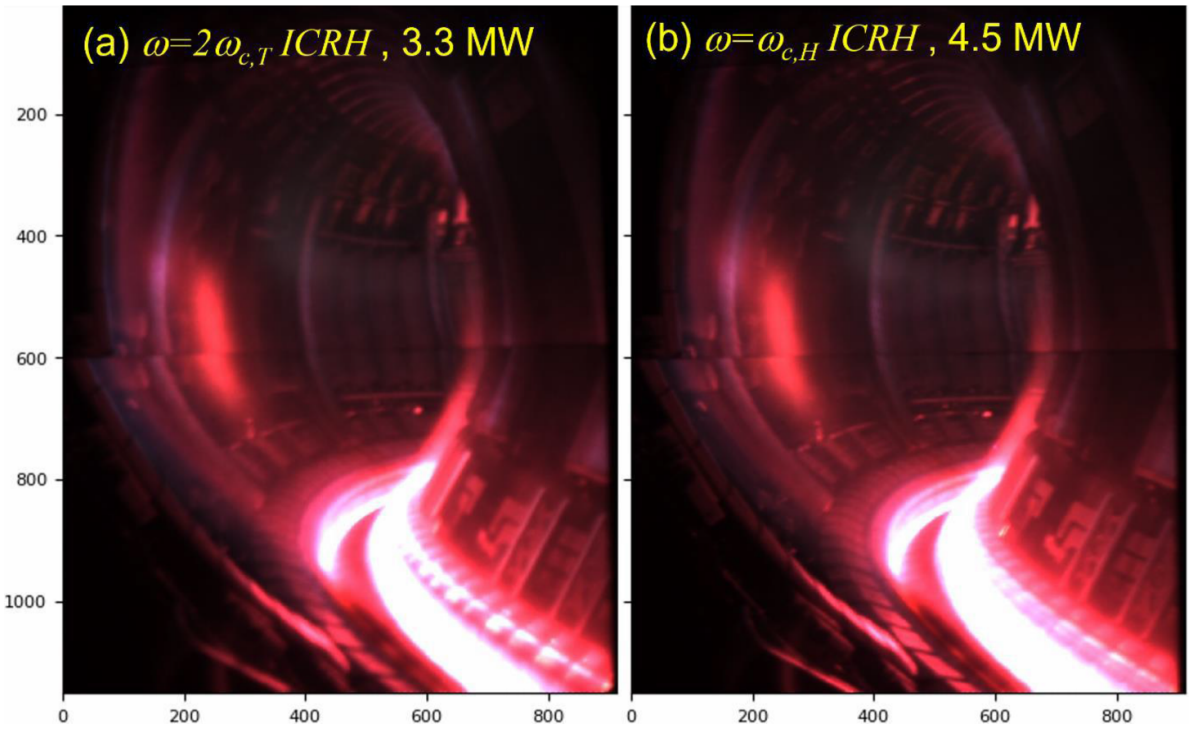

Figure 11. JET in-vessel camera images at $t \sim 10.95$ s for two identical JET DT pulses heated with ∼13.0 MW of D-NBI and ∼13.0 MW of T-NBI and with (*a*) pulse 99886 with $\omega = 2\omega_{c,T}$ ICRH in the centre ($f_{ICRH} = 32.5$ MHz) no resonance on the inner wall; (*b*) pulse 99596 with $\omega = \omega_{c,H}$ ICRH ($f_{ICRH} = 51$ MHz) $P_{ICRH} = 4.5$ MW with $\omega = 2\omega_{c,T}$ resonance on the inner wall. No inner wall heating can be detected even in the case (b) with resonance on the inner wall. Reproduced from [54]. © 2024 Crown copyright, UK Atomic Energy Authority. CC BY 4.0.

DIII-D wall mock-up, first experiments after installation in the machine itself are expected for 2024.

8. Fuel cycle and tritium operation

King *et al* provided a summary about the preparations for, the execution of, and the lessons learnt from the JET tritium and deuterium—tritium campaigns during 2021 and the beginning of 2022 [41], with most features of course already contained in specific publications elsewhere. Bottom line, it can be concluded that the preparation, not only in terms of the upgrade and re-commissioning of the Active Gas Handling System, but also w.r.t. review of operational procedures as well as staff training and rehearsals well in advance of the campaigns combined with refresher trainings close to the actual tritium operation turned out very valuable. Capture of lessons learned was done in a systematic way, which did not only facilitate grouping of issues and follow-up actions, but also triggered individual awareness. Practical outcomes were the usefulness of exercising critical systems on days without tritium operation in order to detect and resolve issues, redundancy for essential diagnostic systems for plant reliability, and having back-up experiments ready and being prepared to change the programme at short notice. It was also found that the focus on pulse budgets w.r.t. tritium use and neutrons in the end was not efficient, as the pre-defined limits were reached only in few cases, and that the original, session-based planning in most cases is more favourable. Furthermore, the use of deuterium in the NBI system turned out more favourable than the use of tritium, as T NBI was less reliable and more restrictive than D NBI—thus removing a long restart phase with T NBI for the DTE3 campaign later in 2022.

The design process for the UKAEA H3AT (Tritium Advanced Technology) Facility from the review of the pre-existing conceptual design up to the stage of procurement & manufacturing readiness, that had been contracted to the company Atkins, was illustrated by Tucker [57]. The facility will have two major operational objectives, i.e. simulate a fully functional tritium fuel cycle loop for fusion facilities, and provide mixtures of tritium gases for future research programmes that can be carried out in an adjacent research hall. As a key element of the design process, a process simulation model was developed with materials databases and component representations. Repeated runs revealed two critical safety issues, i.e. loss of containment and tritium release from two subsystems in the tritium cycle, i.e. the Palladium Membrane System for in-cycle hydrogen purification and the Air Detritiation System for removing tritium from the vented air, which then both could be managed by introducing passive safety systems. S. Bickerton summarized the characteristics of the H3AT tritium loop currently under development [58]. It is meant to be a closed loop at pilot-plant scale and capable of continuous operation, that shall allow developing tritium processing capabilities and support future experiments. In particular, it will contain a scaled-down representation of the ITER

Tritium Plant. Major objectives besides continuous operation, which would not be required for ITER but will be necessary to support continuous plasma operation in future devices, are good control of the fuelling feed quality in terms of control of feed rate and gas composition, minimising tritium losses, as well as the development of tritium extraction processes to make available the tritium to be generated in the breeding blanket. A particular goal is the development and demonstration of a safe fuel cycle architecture through engagement with regulatory bodies.

Modelling of the Fuel Cycle of a tokamak reactor was advanced at the Kurchatov Institute as shown by Ananyev [59]. ASTRA and SOLPS4.3 codes for core and edge plasma simulation were coupled to the FC-FNS code for particle flow simulation via parameterization and integrated into an efficient work flow. This was applied to variants of the Fuel Cycle for the planned FNS-ST compact spherical tokamak neutron source, resulting in total tritium inventories ranging from 90 g to 220 g, depending on the gas purification and pellet injection systems applied and their modes of operation. Applying the same approach with optimized core plasma calculations, i.e. applying ions equations instead of electrons equations, and considering particle losses through convective ELMs as well as compensating pellet injection from the high field side, to a DEMO-FNS system with 40 MW fusion power, yielded a total necessary tritium inventory of ∼800 g, including initial loading, reserves for repair and maintenance, capacity for ELM particle loss compensation, and necessary long-term storage. Furthermore, it was found that depending on the actual degassing rate from the vacuum vessel under steady-state operation, the foreseen pumping capacity (∼30 m^3 s^{-1}) could become marginal or even insufficient.

9. Tritium breeding blanket technologies

At the Brasimone centre of ENEA, an ensemble of facilities for preparing the design and operation of water-cooled lithium-lead (WCLL) tritium breeding blanket test modules for ITER (ITER-TBM) and the full DEMO blanket is currently being set up. As reported by Arena *et al* [60], the W-HYDRA (Water thermal HYDRAulic) experimental platform shall combine three facilities: the water loop (WL), a medium-scale facility to provide pressurized-water-reactor conditions for testing mock-ups of the WCLL ITER-TBM and the DEMO blanket, the STEAM facility for exploring and complementing the critical component of the WCLL energy conversion system, the steam generator, and the PbLi facility LIFUS5/Mod4 for the investigation of the PbLi-water interaction (figure 12).

A number of thermal-hydraulic and thermo-mechanical simulations have been done in order to either confirm or optimize the detailed design of the facilities now under construction, with commissioning and first results w.r.t. EUROfusion blanket concept selection process foreseen in the first quarters of 2025. A particular challenge is the pulsed operation of a tokamak reactor, different from any existing power plant with water cooling. Thus, special care is being given to the inlet and outlet temperatures and pressures of the blanket mock-ups in the WL, because there could be under- and over-pressurization at the beginning and the end of each plasma dwell phase. The effectiveness of the mitigation systems foreseen (electrical heater, spray-depressurization) has been established by in-depth simulations. Furthermore, the pipe & vent design was optimized w.r.t. degassing during filling and the speed of draining procedures. For the STEAM facility, the uniformity (within ±1%) of the flow distribution in the steam generator was confirmed, and the analysis of potential vibration-induced issues yielded no to very little risk in the three areas that had been identified as critical. For the PbLi facility LIFUS5/Mod4, which reproduces the PbLi loop of the ITER WCLL TBM except the recirculation pump, the simulation of the fill and drain procedures resulted in the relocation of the recirculation tank to a lower position in order to avoid an up and down path for the liquid metal in the pipe forest.

Smolentsev *et al* reported remarkable advances in the modelling of liquid metal breeding blankets, in particular w.r.t. the liquid metal flow under the influence of high magnetic fields, temperature gradients and gravity [61]. The approach relies on the combination of the 'consistent and conservative scheme' of iterating flow distributions with efficient elliptic solvers, code integration and use of modern supercomputers. It allows considering the entire blanket instead of model sections only, and enables access to parameter regimes that are blanket-relevant but so far could be approached with huge uncertainties only. The scheme was implemented in parallel in the US HIMAG and the Chinese MHD-UCAS computational solvers for liquid-metal magneto-hydrodynamic flow patterns. The approach was thus applied to the US Dual Coolant Lithium Lead blanket as well as for the Chinese 'dual functional PbLi' blanket. While the results confirmed many conclusions from earlier studies, some aspects obviously will have to be revisited. E.g. it was found that a reversed flow can develop in the buoyancy-assisted upward poloidal flow in the liquid metal front ducts facing the plasma, which so far had been predicted only for the buoyancy-opposed rear ducts. Moreover, the new scheme allows a higher degree of multi-physics integration and thus also predictions on the structural design. In result, it was found that for the blanket concepts considered, the critical interface temperature of 470 °C for the onset of massive corrosion of the RAFM steel exposed to PbLi could be exceeded in some exposed positions.

A new optimization method for the tritium breeding ratio (TBR) in the breeding blanket (MCINO), developed at the South-Western Institute for Physics (SWIP), was presented by Qu *et al* [62]. It uses geometry, materials and neutron source information to establish 3D neutron transport and energy distribution, and provides the local TBR as a function of the input parameters, i.e. allows optimization through algorithms. For verification, the method was applied to two different Chinese configurations of a helium-cooled ceramic breeder blanket, yielding better TBR values in either case.

Kobayashi *et al* showed a new method, developed at NIFS together with Japanese and Thai universities, for detecting both fast neutrons and tritium atoms generated via the $^6Li(n,\alpha)^3H$ reaction in a breeding blanket environment with a single, small-sized detector [63]. It is based upon a

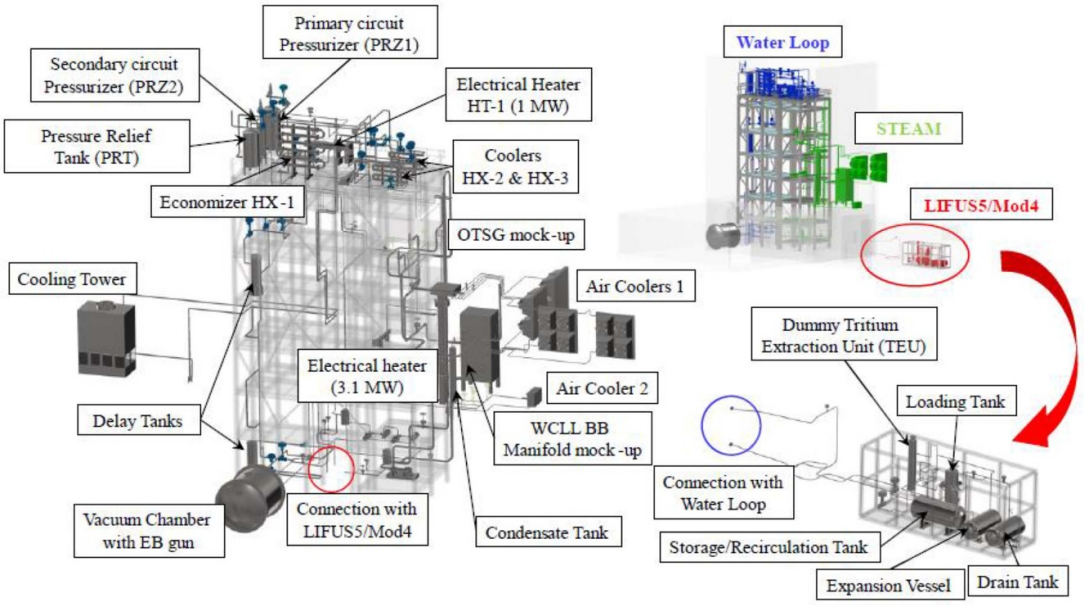

Figure 12. W-HYDRA platform with details of the different components (top right figure: WL in blue, STEAM in green, and LIFUS5/Mod5 in red). Reproduced from [60]. © 2024 The Author(s). Published by IOP Publishing Ltd on behalf of the IAEA CC BY 4.0.

single-crystal CVD diamond disk as detector volume, and the analysis of the pulse shape of the electrical signal generated by the energetic particles. In the validation experiments, a DT neutron source was used, and a polymer foil with a LiF deposit enriched in ^{6}Li simulated the breeder material, and the results obtained were consistent with neutron and ion transport calculation employing the MCNP6 and PHITS.

Predicting the TBR of any particular breeding blanket arrangement requires exact knowledge of the ^{6}Li:^{7}Li isotopic ratio, as the two isotopes have very different energy-dependent reaction rates with neutrons resulting in T production. P. Goswami presented a new, highly precise method for establishing the isotope ratio for natural and ^{6}Li enriched samples [64].

W.r.t. testing mock-ups and prototypes of helium-cooled breeding blankets and divertors as well as other components like lithium–helium heat exchangers, a new high-temperature, high pressure helium loop (design values: 450 °C, 100 bar; flow rate: 0.2–0.45 kg s^{-1}) has been built and commissioned at IPR India as shown by B.K. Yadav [65].

10. Fusion neutron sources

Several contributions highlighted the progress made with the Linear IFMIF (International Fusion Materials Irradiation Facility) Prototype Accelerator (LIPAc) currently under stepwise commissioning in Rokkasho, Japan, in the frame of the Broader Approach agreement between Europe and Japan (figure 13, [66]). LIPAc shall demonstrate the production of a stable, CW deuteron beam of 125 mA up to a deuteron energy of 9 MeV, as a preparation for IFMIF, where a 40 MeV deuteron beam of the same current will be used to produce 14 MeV neutrons when impacting a flowing lithium target. These neutrons then will be used to simulate the neutrons produced in a fusion reactor, in the first instance for materials qualification.

Akagi *et al* reported on the status of the deuteron injector, which is required to produce 140 mA of a D^+ beam at 100 keV with low emittance [67]. The injector consists of an electron cyclotron resonance (ECR) ion source, a low energy beam transport line and a number of diagnostic elements. Beyond the injector, the entire LIPAc includes a radio frequency quadrupole (RFQ) accelerator, a medium energy beam transport line (MEBT), a superconducting radio frequency (SRF) linear accelerator up to 9 MeV, a high energy beam transport line (HEBT) and a beam dump (BD). In pulsed mode operation, the injector had already achieved 160 mA D^+ output at nominal energy; the challenge is now to arrive at CW operation with low emittance and without arcing. Several 'plasma electrodes' (i.e. ring electrodes at the exit of the ECR ion source) have been tried in long-pulse operation, narrowing down the aperture to the range between 11 and 12 mm diameter, in a trade-off between current and emittance (both higher for the larger electrode). A current above 150 mA has now been achieved with an 11.5 mm diameter electrode in CW operation with sufficiently low arcing; however long-term stability still can be an issue. The next system under commissioning is the RFQ accelerator, and the status thereof was shown by De Franco *et al* [68]. RF conditioning and beam experiments with H^+ or D^+ ions are done in exchange. With 80% of nominal vane voltage, CW conditioning of the RFQ had been achieved earlier. This RFQ is the longest ever operated, with a length of 9.8 m. Field perturbations occur along the length due to temperature divergence, and could be compensated by separating cooling water circuits and adjusting their temperatures. RF commissioning with higher voltage had been interrupted then due to arcing in one RF chain circulator, and overheating of O-rings sealing

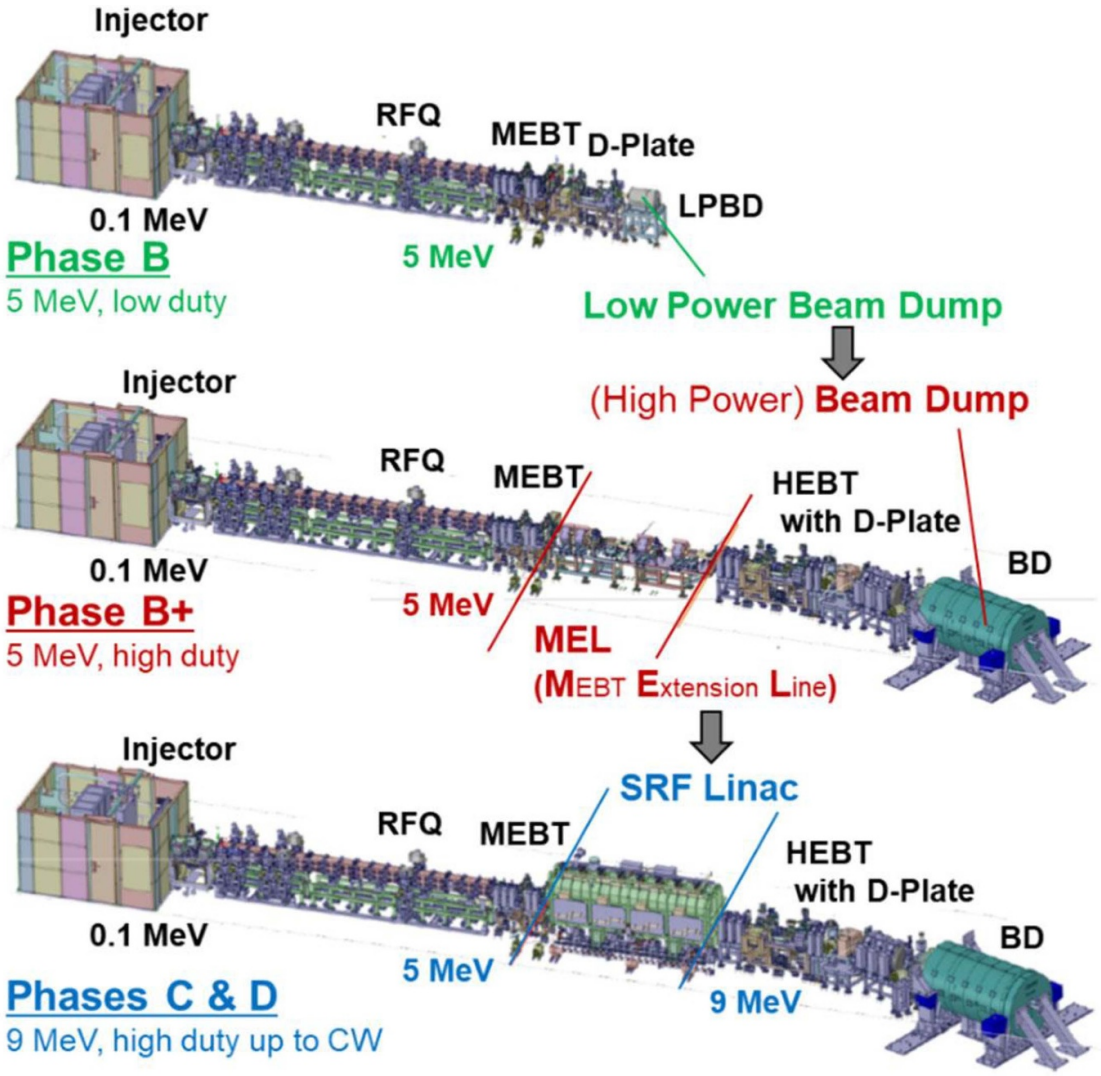

Figure 13. Three different layouts for the stepwise installation and beam commissioning of the LIPAc. Reproduced with permission from [66].

the ceramic vacuum windows of RF couplers. The components were exchanged after re-design, and RF commissioning could be resumed. By the time of reporting, a duty cycle of 7% at nominal vane voltage had been achieved. For the beam commissioning up to 5 MeV, i.e. before installation and commissioning of the SRF linear accelerator, a first phase with 'pilot beams' 10 mA H^+ and 20 mA D^+ ions had been conducted after the exchange of the failed components for a safe start-up and testing of the newly installed elements, as reported by Masuda *et al* [66]. In the next step, the D^+ ion beam is being increased towards the nominal value of 125 mA in low duty cycle. At the stage of reporting, 112 mA in 120 μs pulses at 1 Hz repetition rate had been achieved. Goals are validating the components operated so far including the beam diagnostics, and characterizing the properties of the beam to be injected into the SRF linear accelerator, including verification of simulations. Cismondi *et al* summarized the translation of experiences made during LIPAc commissioning into the next steps [69]. Based upon revised/upgraded designs, a new injector and a new RF power supply will be procured. RFQ couplers, beyond the design improvement on temperature distribution already implemented, will be replaced by components with brazed assembly of the ceramic vacuum window discs instead of window assemblies with O-ring sealings. Reliability and operability of the machine will be further improved by exchanging the existing, tailor-made machine protection system by a new one with centralized design and off-the-shelf components for easy integration and maintenance. Furthermore, a database for tracking the location and lifecycle of each piece of hardware is under construction. This is meant to increase efficiency, avoid errors/duplications and overstock, and facilitate the use of the same standard components by different subsystems. As such, it could become a model for new complex projects like DONES.

The liquid lithium as the target for the deuteron beam in IFMIF will be circulated in a closed loop with a heat exchanger removing the remaining energy from the D^+ beam. Obviously, the oil circulating in the heat exchanger will be exposed to γ radiation, from the activated beryllium as the product of the D, Li reaction and from corrosion products in the liquid lithium

from steel piping and enclosures, activated by the D^+ beam. Tidikas *et al* showed some model calculations with a Monte Carlo method based photon transport code [70], illustrating that the Be-γ activity most likely will not constitute a problem, that however Mn-54, if contained in the activated corrosion products, could increase the radiation level by more than one order of magnitude.

The planned Japanese 14 MeV neutron source A-FNS is, like DONES in Europe, based upon the IFMIF-EVEDA activity under the Broader Approach agreement between Europe and Japan. Thus, the design of several sub-systems is directly derived from there. Other preparation work is still being conducted under Broader Approach Phase 2, as reported by Kasugai *et al* [71]. Recent achievements are establishing the safety conditions for lithium operation, i.e., air atmosphere with less than 0.15 vol% water, and an accident analysis w.r.t. the release of tritium that can be generated from the reaction of the neutrons with the lithium target. Above this, specific developments have been pursued w.r.t. to A-FNS realization in Japan, e.g. the design for an improved high-energy beam transport line for the deuteron accelerator system, maintaining a pressure difference from 1×10^{-9} Pa at the beam entrance to between 1×10^{-3} and 1×10^{-4} Pa at the exit, the latter required to prevent the liquid lithium from boiling. Another important achievement is the design of a test module for DEMO diagnostic elements irradiation in a wide range of neutron fluxes as expected for the real DEMO conditions. Candidate site for A-FNS is an area adjacent to the Rokkasho Fusion Institute, with the idea to enable multi-purpose neutron use beyond fusion, i.e. also for medical, agriculture and semiconductor applications.

Q. Yang provided an overview on the 'family' of HINEG ('High Intensity Steady Neutron Generator') neutron sources [72], with HINEG-Ia, a D–T fusion neutron generator with a flux of 6.4 10^{12} n s^{-1} already in operation. A mock-up experiment towards the Dual Functional Lithium-Lead ITER-TBM was done to validate tritium breeding performance, determine materials activation levels and compare with the results of the 3D neutronic simulation tool TopMC. Further facilities under construction (HINEG-Ib) or in the design process (HINEG-IIb) are cyclotron-based (10^{14} n s^{-1} and 10^{15} n s^{-1} target fluxes, respectively). HINEG-IIb, also under construction, is a high-voltage electrostatic accelerator-based D–T source aiming at 10^{15} n s^{-1}. HINEG-III, targeting a flux of 10^{17}–10^{18}, is in the conceptual design phase.

A different approach for a fusion neutron source was presented by Kargaryan *et al* [73]. Inertial Electrostatic Confinement Fusion means ionizing fuel gas by a high voltage electrostatic field in cylindrical or spherical geometry with the negative electrode in the centre. Collisions among the accelerated ions, or among ions and background atoms, then bring about the fusion reactions. The centre electrode has to be actively cooled to prevent it from melting. Thus, the Iranian Electrostatic Confinement Fusion (IR-IECF) device has been realized as a compact, transportable fusion neutron source.

11. Neutronics

A landmark neutronics experiment was carried out using the 2021 JET DT campaign for fusion neutron exposition of ITER-representative materials samples, and presented by Packer *et al* [74]. Although the overall flux of 14.1 MeV neutrons accumulated during that campaign was a factor of $\sim 10^6$ lower that what is expected in ITER over its anticipated lifetime, the results gave highly important insights in the 'real materials' nuclear responses to fusion neutron exposition. A total of 68 samples was exposed in the long-term irradiation station of JET, receiving neutron fluxes during DT plasma pulses with a factor of $\sim$10 from the expected fluxes during ITER pulses. Materials samples were from ITER TF and PF structural materials, EUROFER 97 to be used in Test Blanket Modules, W and CuCrZr materials from divertor components, 316L stainless steel foreseen for the standard blankets, as well as from vacuum vessel forging mock-ups. They were co-exposed together with neutron dosimetry diagnostics foils and neutron spectrometry diagnostics, as well as samples for positron annihilation spectroscopy, in order to precisely account for the neutron exposure. After irradiation, the nuclear response, discerning 16 radionuclides that had formed during exposition, was determined by means of gamma spectrometry measurements done at five European post-irradiation laboratories besides the UKAEA Materials Research Facility, and compared to calculation results obtained with the inventory code FISPACT-II linked to MCNP radiation transport calculations. In result, many calculations could be confirmed within a calculation/experiment ratio close to 1 (^{46}Sc, ^{51}Cr, ^{54}Mn, ^{59}Fe, ^{95}Nb, and ^{181}Hf), but there was also a significant number of cases with clear deviations like ^{58}Co formed in CuCrZr with a calculated over-estimation of a factor of $\sim$8 (figure 14). Less pronounced overestimations were fond for ^{60}Co, ^{95}Zr, ^{181}W, and ^{185}W in some materials. As the cause for these discrepancies, uncertainties in materials composition certificates can be assumed, together with a possible overestimation of the thermal neutron flux in the JET MCNP model. A particular 'lesson learned' is about the anomalous presence of ^{65}Zn in many samples. This could be traced back to deposits of Zn on the samples during the sample preparation process by Electrical Discharge Machining utilizing a brass (i.e., copper & zinc alloy) wire. As a consequence, new samples for the latest JET DT campaign underwent surface polishing after preparation.

The 2021 JET DT campaign along with the 2020/21 DD and TT campaigns was also used for experiments to validate neutron transport codes using models developed at ORNL, as well as shut-down dose rate calculations, as summarized by Loughlin *et al* [75]. Detailed calculations of this kind are required to design shielding, to provide levels of radiation to which equipment needs to be qualified and validating methods used for safety submissions, and, of course, ensure the protection of workers, the public and the environment. For the neutron streaming, the results in terms of calculation/experiment (C/E) ratio ranged between 0.5 and 2.7, with larger deviations

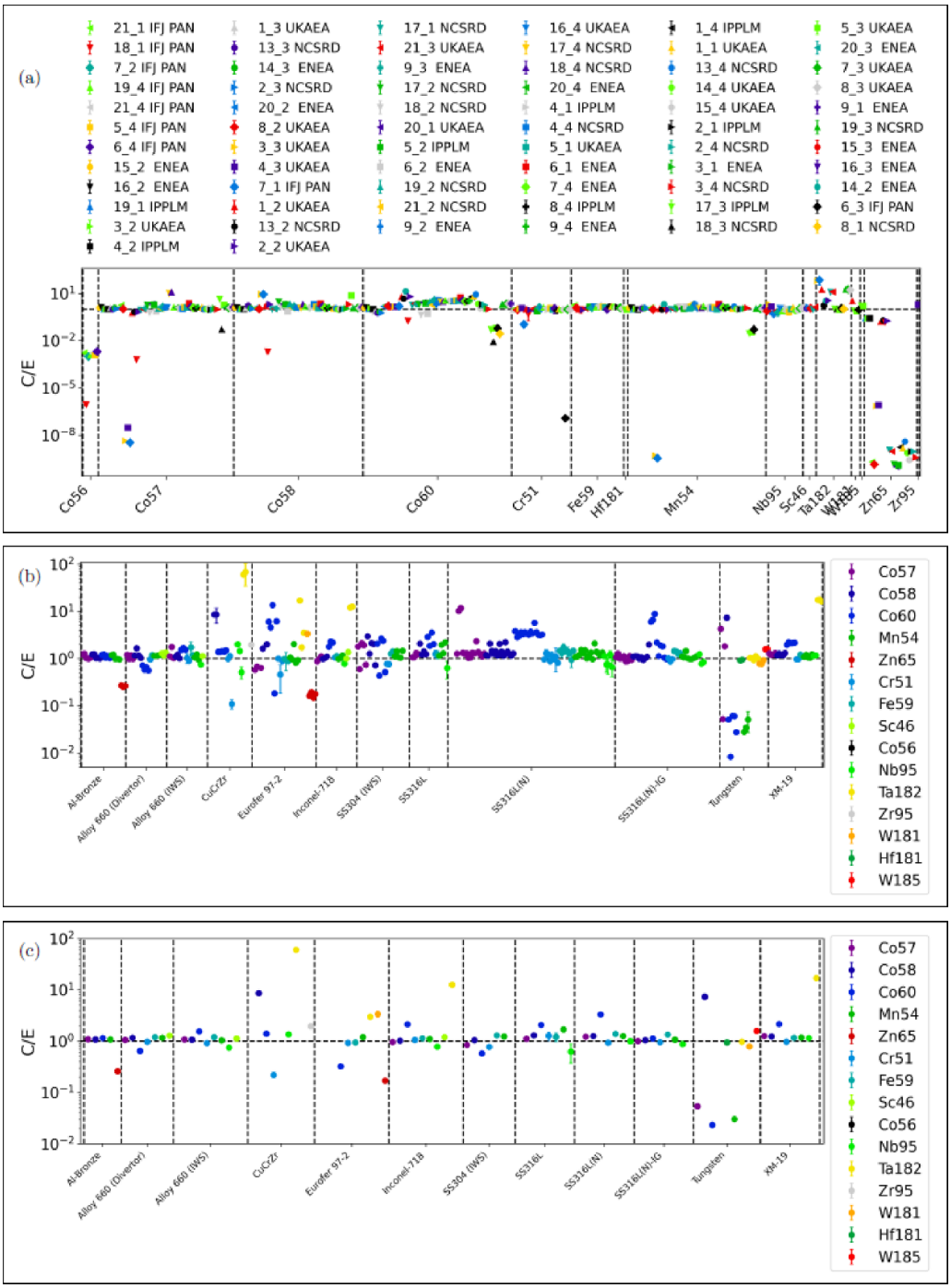

Figure 14. γ activity *C/E* values for measured and calculated ITER materials: *(a)* all results grouped by measured isotope. The legend indicates the position–depth ID; *(b)* all results grouped by material type. *(c)* Weighted average results by material type. Reproduced from [74].

from unity with lower fluence. As a consequence, the authors recommend including an uncertainty factor of 3 in future calculation results. For the shut-down dose rates, *C/E* values where within a 30% margin of unity, thus demonstrating that this important figure can be predicted with reasonable accuracy (figure 15). Still, there are trends in the data which are not yet fully understood, are subject to further investigations, and may allow to further increase prediction accuracy once clarified.

Hill *et al* provided an overview on the IAEA activities on generating and making accessible fundamental data for fusion [76] and gave some examples. Among the recent and ongoing IAEA Coordinated Research Projects (CRPs), the one on 'Data for Atomic Processes of Neutral Beams in Fusion Plasma' on the interactions that neutral particles undergo with plasma ions yielded a new, ∼30% higher cross section for the proton-impact ionization process for H in its ground 1 s state. A benchmark comparison of seven neutral beam

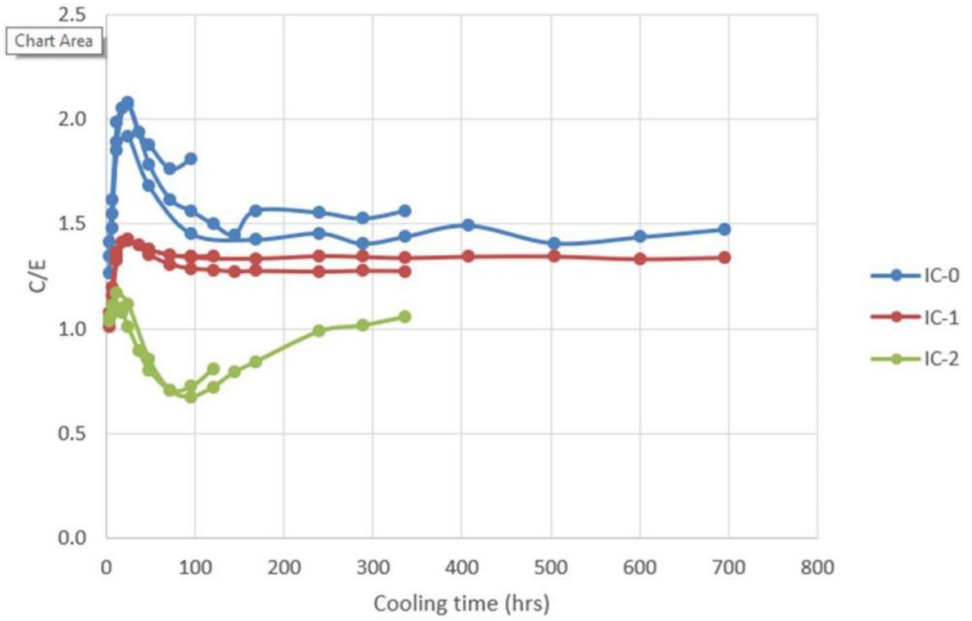

Figure 15. C/E values for JET DT campaigns and three ionization chambers. Reproduced with permission from [75].

penetration and photoemission codes showed good agreement for the beam attenuation, however significant differences in the treatment of photoemission of impurities. In particular, none of the codes provides satisfactory results for the tungsten impurity emission, i.e. further work will be needed here. The ongoing CRP on 'Hydrogen Permeation in Nuclear Materials' aims to address the gap in data on the absorption, diffusion, trapping and transport of hydrogen in fusion reactor candidate materials, particularly, but not only, EUROFER97 and tungsten (figure 16). From among the five databases curated by the IAEA Atomic and Molecular Data Unit, examples of recent developments were given for 'CollisionDB' (collisional and plasma–material interaction (PMI) data), 'CascadesDB' (molecular dynamics simulations of collisional cascades in fusion-relevant materials) and 'DefectDB' (density functional theory calculations of radiation-induced defects in nuclear-relevant materials).

Results of recent activation assessment calculations for the European DEMO tritium breeding blanket concepts were shown by Bailey *et al* [77]. As a general observation, nuclide-specific activation levels depend on the location within the component, i.e. separability of different regions could contribute substantially to reducing waste disposal needs. Furthermore, operation scenarios were shown to have an impact on the results, i.e. have to be taken into account when optimizing a component w.r.t. activation levels and waste volumes. Specifically, ^{60}Co and ^{94}Nb levels in the EUROFER of the Water-Cooled Lithium Lead blanket concept were considered in detail, with the result that the influence of water moderation on the neutron energy results in the ^{60}Co activity at the blanket rear part becoming much more critical than the ^{94}Nb activity. Another important result is that decay heat has to be considered independently, i.e. even when the low-level limit of activities has been reached for all nuclides after some decay time, it still can be that decay heat production will prevent disposal. As an example, tritium production in the breeder material KArlsruhe Lithium OrthoSilicate in the helium-cooled pebble bed (HCPB) concept is such that with 99% depletion/extraction, decay heat would reach the disposal limit, as derived from container specifications by the UK Nuclear Waste Services, after 20 years (figure 17). Of course, the produced tritium is meant to be extracted and used, and with complete tritium recovery, the decay heat disposal limit of the material could be reached within ∼2 years (in reality, there rather will be reprocessing for re-using the unspent lithium).

Wu *et al* presented validation experiments for an improved version of the multi-purpose neutronics code SuperMC originally developed at INEST [78]. The new version, TopMC, now combines electron with neutron/photon transport, allows direct one-step shut-down dose rare calculation, and includes physical parameters visualization. A prominent validation run described is the neutronics analysis of the European DEMO with HCPB blanket, including neutron wall loading, TBR, nuclear heating and radiation loads on the first walls, divertor and TF coils. TopMC results showed good agreement with other codes, including the newly developed methods and functions, while allowing faster calculations with less computer power. Another neutronics code validation, concerning a code developed at Nucleon Power Inc., was presented by Young *et al* [79]. The Milonga code is a free and open-source neutron transport code with unstructured grids, aiming at the optimization of moderator, shielding and activation samples placement in neutron sources for optimum use of the neutrons, e.g. for radio-isotope production, at minimum leakage. Validation was done comparing iteratively code-optimized configurations with experimental results from the D–D fusion based neutron generator Gemini-01. Both for moderator performance and for the optimization of the positioning of Mo–In foils for ^{99}Mo production, good to excellent agreement

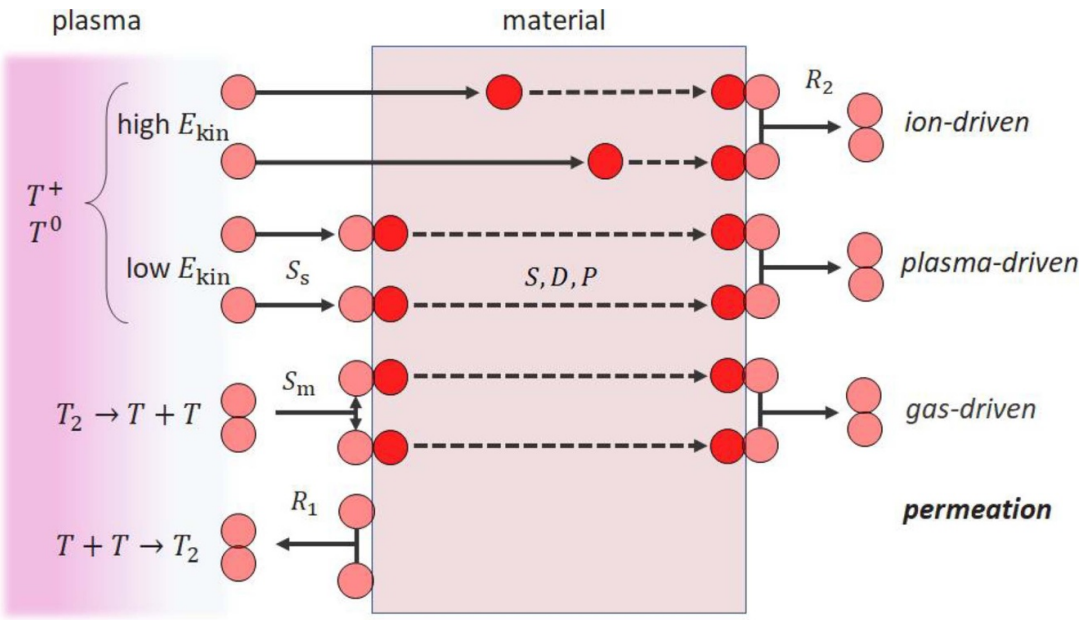

Figure 16. Schematic illustration of energetic (E_{kin}) hydrogen particles (T^0, T^+, T_2) interacting with a plasma-facing material and examples of processes studied in the CRP on hydrogen permeation: sticking ($S_{s,m}$), recombination (R), solubility (S), diffusivity (D), permeability (P). Reproduced with permission from [76].

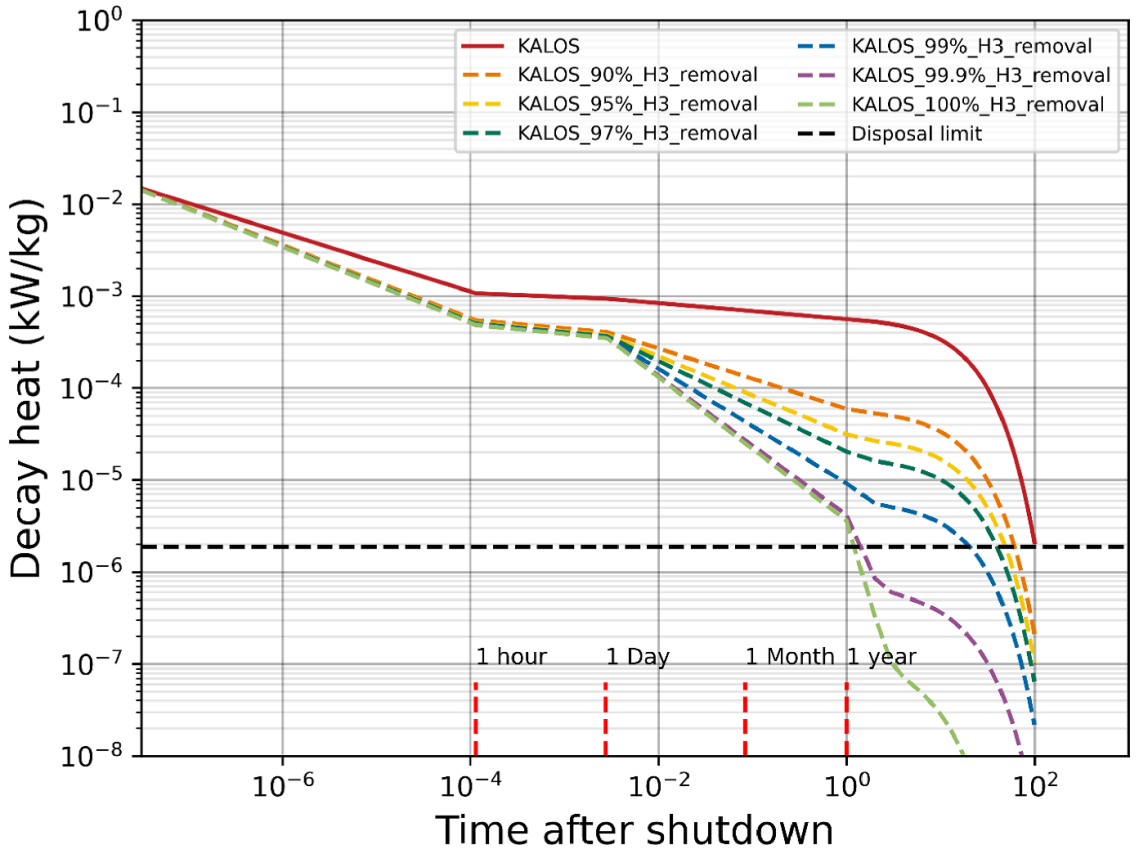

Figure 17. Decay heat of breeding material as a function of tritium removal rate. Time is given in years. Reproduced with permission from [77]. Kanth and Bailey, private communication.

between the optimization calculations and the experiments was found.

12. Technology research devices

After the fault to ground of one of the JT-60SA coils during the 2021 commissioning phase, which had resulted from imperfect electrical insulation, preventive and protective measures were put in place particularly in the areas around the magnets where the electrical insulation could not be changed due to limited access space. These measures, i.e., 'spark wires' (SWs) and 'cold cathode gauges' (CCGs) were presented by Tomarchio [80] and shall ensure to avoid Paschen discharges at the magnets and their feeders, which can occur at vacuum conditions above $\sim 10^{-2}$ Pa at voltages well below the breakdown voltage at atmospheric pressure. SWs are insulated copper wires with deliberately placed openings in the insulation, which would undergo Paschen discharge, if the conditions apply, before the coil systems. CCGs are vacuum pressure detectors based on the Penning principle, which were adapted to the cryo-temperature and magnet field conditions around the coils for providing exact, spatially resolved pressure information in the critical range. The detectors were placed in critical areas of the magnet system and individually adaptable in their voltage. The protection system implies that not a single signal will trigger the ramp-down of the coils, but a minimum number within a given time interval. Before installation in JT-60SA, the detectors successfully underwent a testing and qualification programme. Without reducing the need for effective electrical insulation, the system could be beneficial as an additional safety measure for the expensive, in parts unreplaceable, superconducting magnet systems of future fusion machines.

Measurements during the 2021 commissioning phase of JT-60SA also gave rise to a modelling exercise presented by Zani *et al* [18]. It had been found that the temperature increase at the outlet of the supercritical He coolant when energizing the superconducting coils to nominal current was twice as high for the TF coil No. 2 (TF 02) than for the other TF coils. Due to limited instrumentation inside the cooling circuit, it was not possible to measure the impact of the three suspected, normal conducting joint resistances (feeder to winding pack, pack-to-pack within pancake, winding pack to feeder) between the superconducting coil and feeder cables. Instead, a previously developed model (TACTICS) was applied to simulate the thermal flows along the path of the helium, with the joint resistances as the remaining variable. Thus, the nominal resistances in the feeder joints could be established, and it could be confirmed that, despite the higher-than-nominal resistance, a positive temperature margin remains under commissioning conditions w.r.t. the local transition temperature of the superconductor.

The purpose of the WEST tokamak is studying tungsten PFCs under all possible operation conditions, often requiring to bring them close to their operational limits. Thus, an integral PFC protection system has been developed for, and implemented at, WEST and was presented by Houry *et al* [81]. The system comprises IR detectors, data processing and automated protection measures, organizational measures as well as modelling and deep learning approaches, together with long-term fatigue assessment. The IR thermographic detectors are set up to monitor 100% of the heating systems (ICRH and LH current drive antennas), 1/6 of the vacuum vessel surface via a wide-angle viewing system, and 82% of the divertor surface. For studying the plasma–wall interactions, a high-resolution IR camera as well as a fast IR camera have been developed and installed. Organizational measures include the definition of 'regions of interest' with pre-defined temperature limits not to be exceeded during the plasma discharges, and characterization of the respective components before their installation in the machine. Furthermore, operation requires the presence of one member of the 'Plasma Facing Components Protection Officer Team' in order to allow rapid checking of automated signals and measures for their plausibility in view of the next discharge. Signal processing is to a large extent done close to the cameras, and the Plasma Control System will stop the discharge within a time frame of less than 200 ms if an alarm level is reached. Of course, due to reflections and changes in reflectivity, this could lead to a rather high percentage of prematurely terminated discharges. Thus, methods have been put in place to improve the quality of the automated response via data collection, model generation and deep learning techniques, with particular attention to discriminating reflection patterns from real thermal events (figure 18). W.r.t. thermal fatigue, the wide-angle IR viewing system allows long-term analysis of surface temperature cycling particularly of the water cooling pipes of the upper divertor, which are frequently exposed to extraordinary heating by fast electrons, thus allowing damage rate estimation. All these methods are now being shared with other devices, e.g. Wendelstein 7-X and EAST, and will also help ITER operation in the future.

At the DTT, under construction at ENEA Frascati, the power supply and electrical systems are among the first systems in the procurement process. The particular challenges to be faced, and innovations developed, were presented by Lampasi *et al* [82]. Besides the fluctuating power and protection needs common to all tokamak facilities, the relevant demands for reactive power, the necessary fast dynamic responses, and the balancing of conflicting requirements on the maximum voltage and the minimum time in the fast discharge of the superconducting coils posed particular challenges. The 18 TF coils will be powered by a single power supply, protected, inter alia, by 3 fast discharge units for 3 sectors of 6 coils each, to ensure the same current and magnetic field around the torus. The 6 PF coils, grouped in 3 sets, however will be served by one individual power supply each, with a view of the need for continuous individual current adjustments derived from the prospective operation scenarios. Also, each of the 6 segments of the CS will have an independent power supply. The impact on the external grid will be limited by storing most of the energy in the super-capacitor-based DC links. The electrical design of the in-vessel coils is not complete yet; in any case, there will be three groups of these. Vertical plasma stabilization will be achieved by two identical coils fed by two independent DC/AC multilevel convertors

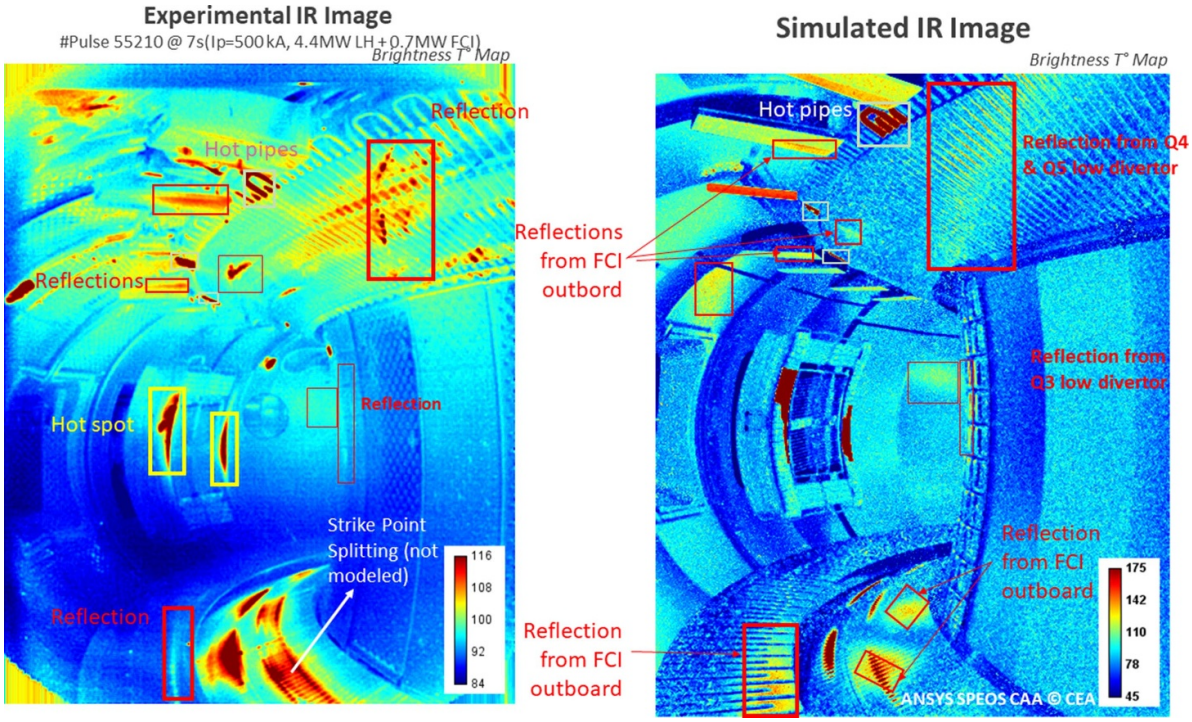

Figure 18. Experimental image (left) and simulated image (right) of WEST wide angle camera. The simulation makes it possible to distinguish the thermal events from the reflection patterns and to determine their origin. Reproduced with permission from [81].

with an output voltage up to 5 kV. For shaping the plasma in the divertor region, 3 or 4 in-vessel coils will be served by 3 independent power supply circuits, and for error field correction and mitigation of edge-localized modes, 3 rows of 3 non-axisymmetric in-vessel coils are foreseen. Besides to the ex-vessel and in-vessel coils, the electrical distribution system has to supply electricity also to the plasma heating systems, which actually represent the most demanding loads with a total of 45 MW discontinuous heating power to the plasma. Thus, the electrical distribution system will be divided into two sections, i.e. a steady-state electrical network and a pulsed power electrical network. A further aspect to note is that the energy stored in the superconducting coils will be discharged by high-energy silicon carbide (SiC) varistors instead of standard resistors, allowing an optimized trade-off between the discharge time, the energy passing through the coils and the peak voltage. Furthermore, most of the pulsed power supplies will use energy-conservation topologies with large supercapacitor banks in the DC-links for recovering the magnetic pulse energy in electrostatic form, and the same couple of vertical stabilization coils in anti-series configuration is able to implement both the vertical stabilization and radial control functions, with a mitigating effect on plasma disruptions.

At CIEMAT, the OLMAT facility has been set up for the investigation of conventional and advanced divertor targets exposed to high power neutral beam and laser irradiation. Oyarzabal *et al* reported on the commissioning of the facility as well as on first results with solid tungsten capillary porous structures (CPSs) filled with tin [83]. The facility can use one of the two neutral beam systems of the stellarator TJ-II with up to 58 MW m^{-2} heat flux, as well as a quasi-continuous IR laser system with 9.3 kW average power and 90 J pulse energy. It has detector systems allowing the investigation of physical phenomena such as vapour shielding, thermal sputtering, the formation/characterization of plasma plumes and the detection of impurities in front of the studied targets. A comparative study of surface-temperature increase and homogeneity, particle ejection, CPS damage and overall behaviour was performed, using the neutral beam system, a fast-frame imaging camera and an IR pyrometer, on four different Sn wetted W CPS targets (figure 19). The results underline the importance of good wetting of the structure (as well as good thermal contact to the substrate), problems with very small pore sizes <1 μm, as well as problems that can arise from crack formation, e.g. in sintered structures. Bottom line the 3D printed W target, containing an internal reservoir for the liquid Sn, showed the best performance. Furthermore, drop formation at the bottom of the targets can give rise to splashing/particle ejection. This observation is in line with effects observed for CPS target structures tested in ASDEX Upgrade, and could be a show-stopper for the use of Sn. In the very first experiments at OLMAT utilizing the IR laser system, ablation on-set for W CPS wetted with Sn at different filling degrees have been obtained. Higher heat fluxes (around 400 MW m^{-2}) are required for the ablation of a pure W surface under such conditions (10 ms laser pulse length). For Sn wetted surfaces, ablation on-set at lower heat fluxes (around 200 MW m^{-2}) was observed.

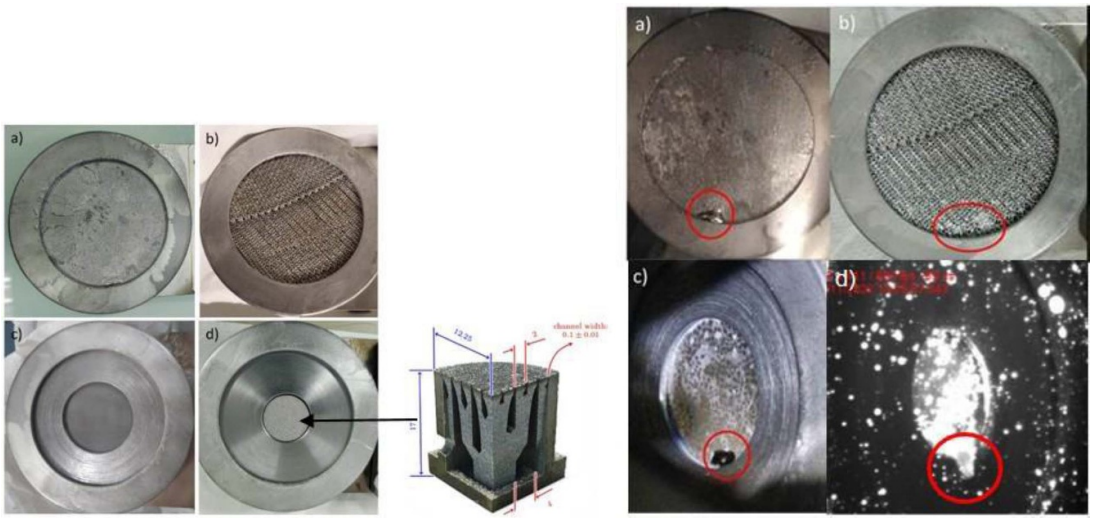

Figure 19. Left: four Sn wetted W CPS targets exposed to OLMAT: W meshes (*a*), W felt (*b*), sintered W disk (*c*) and 3D printed W (*d*); right: drop formation/accumulation of Sn (red circle) at the bottom of the targets. Reproduced with permission from [83].

Tulenbergenov *et al* reported on the set-up of a plasma beam installation (PBI) and on the development of an automatized method for determining plasma parameters that was validated with this device—in support of the Kazakhstan Material Testing Tokamak KTM [84]. The PBI generates a beam plasma discharge and allows the determination of radial plasma particle energy and density distribution via automated calculation from electric probe measurements (in the periphery) and optical emission spectroscopy (in the beam centre). The dependencies found shall allow to establish correlations between the plasma parameters in KTM for materials exposition and the surface processes to be observed, as well as to understand the dynamics of these processes and their plasma parameter dependence.

The Material Plasma Exposure eXperiment (MPEX) is a linear plasma device to test materials, including irradiated materials, to fusion divertor reactor relevant fluxes and fluences currently being set up at ORNL, with a helicon source to generate the plasma, EC heating to heat the electrons and IC heating to heat the ions. Rapp *et al* gave an overview on the digital twin development to accelerate commissioning [85]. The digital twin shall couple and combine RF source and heating models, plasma, neutral and impurity transport models, and PMI models to calculate the plasma and impurity fluxes from MPEX engineering parameters. Comparison of modelling approaches, e.g. COMSOL for RF modelling, SOLPS-ITER for plasma transport, or WALLDYN for studying impurity transport, with experimental results obtained with the Proto-MPEX facility, yielded reasonable agreement.

Raj *et al* reported on the progress at IPR India towards magnets based upon high-temperature superconductors (REBCO) [86]. A solenoid coil with inner bore diameter of 50 mm and a field of up to 1 T, operating at 77 K, has been realized and tested down to 10 K. A prototype D-shaped coil is under manufacturing, aiming at a toroidal configuration of eight such coils with 30 windings each, which should produce a field of 0.1 T at a major radius of 0.5 m. At SWIP, a high-temperature superconductor cable and strand has been developed and tested in view of the TF coil of a compact fusion reactor, as shown by Li *et al* [87]. The cable-in conduit conductor approach was taken with stacked YBCO tapes, with a filling solder of $Sn_{63}Pb_{37}$ as an innovative, new element. The solder, applied via a vacuum pressure impregnation and extrusion process, serves to increase mechanical strength and to reduce stress on the tape stacks. Due to its low melting temperature, the critical current density of the superconductor is not decreased during manufacturing. Intense testing after mechanical loading confirmed that the conductor cable and strand are mechanically strong enough for the intended application in fusion magnets, while the in-depth electromechanical testing was still in progress at the time of reporting.

The fusion virtual reality cave facility AABHAS, established at IPR India, was presented by Rastogi *et al* [88]. It is compatible with numerous design and simulation software platforms and allows 3D virtual walkthroughs of machines, accurate virtual prototyping, system interface & integration studies, real-time monitoring and control of RH operations and customized operator training. In particular, its novel aspect is the real time monitoring and control of remote maintenance operations, allowing operators to visualize and interact with the environment as if they were physically present.

13. Conclusions

The 29th IAEA Fusion Energy Conference provided an excellent overview on the state of development w.r.t. the realization of ITER and of plasma heating systems. For ITER, the achievements and experiences with the manufacturing of the large components, as well as with the safety, diagnostic and control systems were impressive. Remarkable progress also could be seen in the different areas of plasma heating and current drive development, but also the setback suffered at the flagship project, the ITER NBTF, and the lessons taken

thereof. For the nuclear topics, highlights were the reports on the different aspects of the JET DT, DD and TT operation in 2021 and 2022, as well as on the status of the LIPAc, and the lessons learned from the difficulties encountered there. Even more important, the report on the lessons learned, and the measures resulting, from the incident during the 2021 commissioning of JT-60SA, will have a strong impact in the field.

ORCID iD

Klaus Hesch https://orcid.org/0000-0002-9222-1091

References

[1] Bhardwaj A.K. *et al* 2023 Challenges and lessons learnt during manufacturing, transportation and assembly of ITER cryostat *Preprint: 2023 IAEA Fusion Energy Conf.* (*London, United Kingdom, 16–21 October 2023*) TEC/1–4 (available at: https://conferences.iaea.org/event/316/contributions/27792/)

[2] Hemmi T. *et al* 2024 Lessons learned from European and Japanese production of ITER toroidal field coils *Nucl. Fusion* **64** 066010

[3] Kajitani H. *et al* 2024 Completion of all the ITER toroidal field coil structures *Nucl. Fusion* **64** 096026

[4] Bonito Oliva A. *et al* 2023 Lessons learned in the management of the production of the poloidal field coils (and other coils) *Preprint: 2023 IAEA Fusion Energy Conf.* (*London, United Kingdom, 16–21 October 2023*) TEC/1–5 (available at: https://conferences.iaea.org/event/316/contributions/27793/)

[5] Wooley K. *et al* 2023 Lessons learned from ITER central solenoid manufacturing *Preprint: 2023 IAEA Fusion Energy Conf.* (*London, United Kingdom, 16–21 October 2023*) TEC/1–3 (available at: https://conferences.iaea.org/event/316/contributions/27795/)

[6] Lu K. *et al* 2024 Correction coil and magnet feeder lessons learned *Nucl. Fusion* **64** 066033

[7] Lehnen M. *et al* 2023 Physics basis and technology development for the ITER disruption mitigation system *Preprint: 2023 IAEA Fusion Energy Conf.* (*London, United Kingdom, 16–21 October 2023*) TEC/1–1 (available at: https://conferences.iaea.org/event/316/contributions/27794/)

[8] Gebhart T.E. *et al* 2024 Impact of breech geometry and propellant flow on the release of large pellets for the ITER disruption mitigation system *Nucl. Fusion* **64** 036021

[9] Zoletnik S. *et al* 2023 Support laboratory for testing and developing shattered pellet injection components for the ITER disruption mitigation system *Preprint: 2023 IAEA Fusion Energy Conf.* (*London, United Kingdom, 16–21 October 2023*) TEC/P8–13 (available at: https://conferences.iaea.org/event/316/contributions/28691/)

[10] Baylor L.R. *et al* 2023 Progress toward continuous pellet injection systems for fueling of long pulse stellarators and tokamaks *Preprint: 2023 IAEA Fusion Energy Conf.* (*London, United Kingdom, 16–21 October 2023*) TEC/P3–20 (available at: https://conferences.iaea.org/event/316/contributions/28148/)

[11] Aquaro D. *et al* 2023 Performances of the ITER pressure suppression system during unstable steam condensation regimes *Preprint: 2023 IAEA Fusion Energy Conf.* (*London, United Kingdom, 16–21 October 2023*) TEC/P8–14 (available at: https://conferences.iaea.org/event/316/contributions/28689/)

[12] El-Morshedy S.E. 2023 Thermal-hydraulic simulation of ITER tungsten divertor monoblock for loss of flow transient *Preprint: 2023 IAEA Fusion Energy Conf.* (*London, United Kingdom, 16–21 October 2023*) TEC/P1–19 (available at: https://conferences.iaea.org/event/316/contributions/27974/)

[13] Shibama Y. *et al* 2023 Progress and challenges in commissioning operation on JT-60SA tokamak device system *Preprint: 2023 IAEA Fusion Energy Conf.* (*London, United Kingdom, 16–21 October 2023*) TEC/P1–21 (available at: https://conferences.iaea.org/event/316/contributions/27972/)

[14] Roy S. *et al* 2023 Experimental & simulation study on SST-1 PF#3 vacuum barriers arcing incidences and mitigation techniques *Preprint: 2023 IAEA Fusion Energy Conf.* (*London, United Kingdom, 16–21 October 2023*) TEC/P5–19 (available at: https://conferences.iaea.org/event/316/contributions/28471/)

[15] Devlin-Hill B. *et al* 2023 Inspecting the aftermath of vertical displacement events by integrating the JOREK-STARWALL plasma simulation code into a remote maintenance system *Preprint: 2023 IAEA Fusion Energy Conf.* (*London, United Kingdom, 16–21 October 2023*) TEC/P5–18 (available at: https://conferences.iaea.org/event/316/contributions/28470/)

[16] Vives S. *et al* 2023 Design of the visible and infrared wide angle viewing system diagnostic for ITER equatorial port 12 at final design review *Preprint: 2023 IAEA Fusion Energy Conf.* (*London, United Kingdom, 16–21 October 2023*) TEC/P3–18 (available at: https://conferences.iaea.org/event/316/contributions/28146/)

[17] Aumeunier M.-H. *et al* 2024 Surface temperature measurement from infrared synthetic diagnostic in preparation for ITER operations *Nucl. Fusion* **64** 086044

[18] Zani L. *et al* 2023 Development of JT-60SA TF feeder model with tactics tool for support to thermal-thermohydraulic analyses of terminal joint temperature margin *Preprint: 2023 IAEA Fusion Energy Conf.* (*London, United Kingdom, 16–21 October 2023*) TEC/P3–6 (available at: https://conferences.iaea.org/event/316/contributions/28131/)

[19] Joshi J. *et al* 2023 Realization of beam line components for ITER DNB system- lessons learnt *Preprint: 2023 IAEA Fusion Energy Conf.* (*London, United Kingdom, 16–21 October 2023*) TEC/P3–17 (available at: https://conferences.iaea.org/event/316/contributions/28142/)

[20] Muvvala V.N. *et al* 2023 Design development of drift duct for diagnostic neutral beam system of ITER *Preprint: 2023 IAEA Fusion Energy Conf.* (*London, United Kingdom, 16–21 October 2023*) TEC/P8-8 (available at: https://conferences.iaea.org/event/316/contributions/28687/)

[21] Yadav A. *et al* 2023 Design development of nuclear grade vacuum vessel for diagnositc neutral beam of ITER *Preprint: 2023 IAEA Fusion Energy Conf.* (*London, United Kingdom, 16–21 October 2023*) TEC/P3–14 (available at: https://conferences.iaea.org/event/316/contributions/28143/)

[22] Sharma D.K. *et al* 2023 Porcelain based 100 kV feedthrough for prototype ITER DNB at INTF, *Preprint: 2023 IAEA Fusion Energy Conf.* (*London, United Kingdom, 16–21 October 2023*) TEC/P5–14 (available at: https://conferences.iaea.org/event/316/contributions/28467/)

[23] Mattei M. *et al* 2023 Axisymmetric magnetic control in ITER for PFPO-1 *Preprint: 2023 IAEA Fusion Energy Conf.* (*London, United Kingdom, 16–21 October 2023*) TEC/P5–17 (available at: https://conferences.iaea.org/event/316/contributions/28469/)

[24] Mattei M. *et al* 2023 A new design tool for startup in large tokamaks with superconducting coils *Preprint: 2023 IAEA*

Fusion Energy Conf. (*London, United Kingdom, 16–21 October 2023*) TEC/P3–21 (available at: https://conferences.iaea.org/event/316/contributions/28147/)
[25] Portnov D. *et al* 2023 Challenges of integration of diagnostics into nuclear environment *Preprint: 2023 IAEA Fusion Energy Conf.* (*London, United Kingdom, 16–21 October 2023*) TEC/P8–15 (available at: https://conferences.iaea.org/event/316/contributions/28690/)
[26] Mukhin E.E. *et al* 2023 High technologies developed for ITER divertor Thomson scattering and their experimental testing *Preprint: 2023 IAEA Fusion Energy Conf.* (*London, United Kingdom, 16–21 October 2023*) TEC/P3–19 (available at: https://conferences.iaea.org/event/316/contributions/29274/)
[27] Shevelev A.E. *et al* 2023 Combined neutron and gamma-ray spectrometry for ITER *Preprint: 2023 IAEA Fusion Energy Conf.* (*London, United Kingdom, 16–21 October 2023*) TEC/P1–23 (available at: https://conferences.iaea.org/event/316/contributions/29280/)
[28] Gusarov A. *et al* 2023 Progress in the development of the fibre optics current sensor for magnetic fusion devices *Preprint: 2023 IAEA Fusion Energy Conf.* (*London, United Kingdom, 16–21 October 2023*) TEC/P1–15 (available at: https://conferences.iaea.org/event/316/contributions/27967/)
[29] Schissel D.P. *et al* 2024 Remote operation of the DIII-D National Fusion Facility *Nucl. Fusion* **64** 076004
[30] Bruschi A. *et al* 2024 Conceptual design of a modular EC system for EU-DEMO *Nucl. Fusion* **64** 106003
[31] Henderson M.A. *et al* 2023 The concept design of the step HCD system *Preprint: 2023 IAEA Fusion Energy Conf.* (*London, United Kingdom, 16–21 October 2023*) TEC/P8–10 (available at:https://conferences.iaea.org/event/316/contributions/28688/)
[32] Freethy S. *et al* 2024 The optimisation of the STEP electron cyclotron current drive concept *Nucl. Fusion* **64** 126035
[33] Webster H. *et al* 2023 Design and development of an electron Bernstein wave heating and current drive system for MAST-U *Preprint: 2023 IAEA Fusion Energy Conf.* (*London, United Kingdom, 16–21 October 2023*) TEC/P8–12 (available at: https://conferences.iaea.org/event/316/contributions/28684/)
[34] Marsen S. *et al* 2023 Performance of the Wendelstein 7-X ECRH plant during the second operational phase *Preprint: 2023 IAEA Fusion Energy Conf.* (*London, United Kingdom, 16–21 October 2023*) TEC/P3–10 (available at: https://conferences.iaea.org/event/316/contributions/28144/)
[35] Ikeda R. *et al* 2023 Demonstration of triple-frequency gyrotron for ITER and development of gyrotron operation technology *Preprint: 2023 IAEA Fusion Energy Conf.* (*London, United Kingdom, 16–21 October 2023*) TEC/3–3 (available at: https://conferences.iaea.org/event/316/contributions/27831/)
[36] Kariya T. *et al* 2023 Development of MW gyrotrons with collaboration research for plasma heating in fusion experimental devices *Preprint: 2023 IAEA Fusion Energy Conf.* (*London, United Kingdom, 16–21 October 2023*) TEC/P1–12 (available at: https://conferences.iaea.org/event/316/contributions/27963/)
[37] Rao S.L. *et al* 2023 Successful commissioning & demonstration of ITER relevant RF performance (1MW at 170 GHz) at ITER-India gyrotron test facility *Preprint: 2023 IAEA Fusion Energy Conference* (*London, United Kingdom, 16–21 October 2023*) TEC/P8–9 (available at: https://conferences.iaea.org/event/316/contributions/28685/)
[38] Kajiwara K. *et al* 2023 Optical design and prototype tests of the ITER equatorial EC H&CD launcher *Preprint: 2023 IAEA Fusion Energy Conf.* (*London, United Kingdom, 16–21 October 2023*) TEC/P1–16 (available at: https://conferences.iaea.org/event/316/contributions/27960/)
[39] Yamazaki H. *et al* 2023 Development of high-power long-pulse multi-frequency transmission line for the JT-60SA ECH&CD system *Preprint: 2023 IAEA Fusion Energy Conf.* (*London, United Kingdom, 16–21 October 2023*) TEC/P1–17 (available at: https://conferences.iaea.org/event/316/contributions/27961/)
[40] Thackston K.A. *et al* 2023 High frequency dielectric lined waveguides enabling future ECH/ECE in fusion energy development *Preprint: 2023 IAEA Fusion Energy Conf.* (*London, United Kingdom, 16–21 October 2023*) TEC/3–4 (available at: https://conferences.iaea.org/event/316/contributions/27832/)
[41] King D.B. *et al* 2023 Tritium neutral beam injection on JET: calibration and plasma measurements of stored energy *Nucl. Fusion* **63** 112005
[42] Toigo V. *et al* 2023 Experimental results and activities for the optimisation of the ITER neutral beam injector prototypes *Preprint: 2023 IAEA Fusion Energy Conf.* (*London, United Kingdom, 16–21 October 2023*) TEC/P8–11 (available at: https://conferences.iaea.org/event/316/contributions/28686/)
[43] Marconato N. *et al* 2023 Integration of new sets of magnets for improved plasma confinement in the SPIDER experiment *Fusion Eng. Des.* **193** 113805
[44] Ichikawa M. *et al* 2023 Progress of electrical and nuclear safety design of DC 1MV power supply for the ITER neutral beam injector *2023 IAEA Fusion Energy Conf.* (*London, United Kingdom, 16–21 October 2023*) TEC/P1–11 (available at: https://conferences.iaea.org/event/316/contributions/27966/)
[45] Fantz U. *et al* 2024 Contributions of the extended ELISE and batman upgrade test facilities to the roadmap towards ITER NBI *Nucl. Fusion* **64** 086063
[46] den Harder N. *et al* 2024 Beam optics of RF ion sources in view of ITER's NBI systems *Nucl. Fusion* **64** 076046
[47] Nakano H. *et al* 2023 Radio frequency discharge effects on negative ion source for neutral beam injector *2023 IAEA Fusion Energy Conf.* (*London, United Kingdom, 16–21 October 2023*) TEC/P1–18 (available at: https://conferences.iaea.org/event/316/contributions/27962/)
[48] Tobari H. *et al* 2023 Progress on long-pulse and ITER-relevant-intensity negative ion beam accelerations for ITER neutral beam injector *Preprint: 2023 IAEA Fusion Energy Conf.* (*London, United Kingdom, 16–21 October 2023*) TEC/4–5 (available at: https://conferences.iaea.org/event/316/contributions/27846/)
[49] Osei-Mensah W. *et al* 2023 Radiation responses in a neutral beam injector guard wall of the ITER using MCNP6 and GEANT4 *Preprint: 2023 IAEA Fusion Energy Conf.* (*London, United Kingdom, 16–21 October 2023*) TEC/P1–10 (available at: https://conferences.iaea.org/event/316/contributions/27965/)
[50] Sha M.A. *et al* 2023 Influence of wall on plasma transport across magnetic filter field in a negative ion source: a 2D-3V PIC MCC simulation study *Preprint: 2023 IAEA Fusion Energy Conf. (London, United Kingdom, 16–21 October 2023) TEC/P5-12* (available at: https://conferences.iaea.org/event/316/contributions/28468/)
[51] Pandya K. *et al* 2023 Influence of confinement magnets on negative ion source performance *Preprint: 2023 IAEA Fusion Energy Conf.* (*London, United Kingdom, 16–21 October 2023*) TEC/P3–16 (available at: https://conferences.iaea.org/event/316/contributions/28141/)
[52] Hopf C. *et al* 2024 Decoupling beam power and beam energy on ASDEX Upgrade NBI with an *in-situ* variable extraction gap system *Nucl. Fusion* **64** 096017

[53] Jha A. *et al* 2023 200 kW, 1 MHz dual directional coupler: design and characterization *Preprint: 2023 IAEA Fusion Energy Conf.* (*London, United Kingdom, 16–21 October 2023*) TEC/P3–15 (available at: https://conferences.iaea.org/event/316/contributions/28145/)
[54] Jacquet P. *et al* 2024 ICRH operations during the JET tritium and DTE2 campaigns *Nucl. Fusion* **64** 066039
[55] Helou W. *et al* 2023 The ITER ICRF system: latest technological developments, coupling studies and compatibility with high Z wall *Preprint: 2023 IAEA Fusion Energy Conf.* (*London, United Kingdom, 16–21 October 2023*) post deadline paper TEC-HCD (available at: https://conferences.iaea.org/event/316/contributions/29371/)
[56] Wukitch S.J. *et al* 2023 Development of DIII-D high field side lower hybrid current drive launcher *Preprint: 2023 IAEA Fusion Energy Conf.* (*London, United Kingdom, 16–21 October 2023*) TEC/P5–16 (available at: https://conferences.iaea.org/event/316/contributions/28466/)
[57] Tucker G.G. 2023 Engineering design of an advanced tritium facility *Preprint: 2023 IAEA Fusion Energy Conf.* (*London, United Kingdom, 16–21 October 2023*) TEC/P8–7 (available at: https://conferences.iaea.org/event/316/contributions/28678/)
[58] Bickerton S. *et al* 2023 How the fuel cycle loop in UKAEA's new H3AT facility will address key challenges in tritium management for fusion power plants *Preprint: 2023 IAEA Fusion Energy Conf.* (*London, United Kingdom, 16–21 October 2023*) TEC/P5–4 (available at: https://conferences.iaea.org/event/316/contributions/28463/)
[59] Ananyev S.S. *et al* 2023 Progress in modeling D/T component flows in tokamak-based fusion neutron source fueling system *Preprint: 2023 IAEA Fusion Energy Conf.* (*London, United Kingdom, 16–21 October 2023*) TEC/P3–5 (available at: https://conferences.iaea.org/event/316/contributions/29295/)
[60] Arena P. *et al* 2024 W-HYDRA: a new experimental platform for the water-cooled lead lithium breeding blanket *Nucl. Fusion* **64** 076043
[61] Smolentsev S. *et al* 2023 Recent breakthrough in modeling transport processes in a liquid metal blanket *Preprint: 2023 IAEA Fusion Energy Conf.* (*London, United Kingdom, 16–21 October 2023*) TEC/P3–3 (available at: https://conferences.iaea.org/event/316/contributions/27959/)
[62] Qu S. *et al* 2023 MCINO: multi-physics coupling and intelligent neutronic optimization code for tritium breeding blankets of fusion reactors *Preprint: 2023 IAEA Fusion Energy Conf.* (*London, United Kingdom, 16–21 October 2023*) TEC/P8–3 (available at: https://conferences.iaea.org/event/316/contributions/28680/)
[63] Kobayashi M.I. *et al* 2024 Simultaneous measurements for fast neutron flux and tritium production rate using pulse shape discrimination and single crystal CVD diamond detector *Nucl. Fusion* **64** 066026
[64] Goswami P. *et al* 2023 Significance of precise and accurate isotope ratio measurement of lithium *Preprint: 2023 IAEA Fusion Energy Conf.* (*London, United Kingdom, 16–21 October 2023*) TEC/P8–6 (available at: https://conferences.iaea.org/event/316/contributions/28682/)
[65] Yadav B.K. *et al* 2023 Helium cooling system for DEMO R&D *Preprint: 2023 IAEA Fusion Energy Conf.* (*London, United Kingdom, 16–21 October 2023*) TEC/P3–4 (available at: https://conferences.iaea.org/event/316/contributions/28137/)
[66] Masuda K. *et al* 2023 Beam commissioning of linear IFMIF prototype accelerator (LIPAc) toward high-duty operation at 5 MEV, 125 MA D^+ *Preprint: 2023 IAEA Fusion Energy Conf.* (*London, United Kingdom, 16–21 October 2023*) TEC/P1–6 (available at: https://conferences.iaea.org/event/316/contributions/27955/)
[67] Akagi T. *et al* 2024 Achievement of high-current continuous-wave deuteron injector for linear IFMIF prototype accelerator (LIPAc) *Nucl. Fusion* **64** 066005
[68] De Franco A. *et al* 2023 CW conditioning of the high power RFQ and its RF power couplers for the linear IFMIF prototype accelerator (LIPAc) *Preprint: 2023 IAEA Fusion Energy Conf.* (*London, United Kingdom, 16–21 October 2023*) TEC/P1–8 (available at: https://conferences.iaea.org/event/316/contributions/27959/)
[69] Cismondi F. *et al* 2023 Recent linear IFMIF prototype accelerator (LIPAc) maintenance and reliability improvements and future LIPAc upgrades *Preprint: 2023 IAEA Fusion Energy Conf.* (*London, United Kingdom, 16–21 October 2023*) TEC/P3–1 (available at: https://conferences.iaea.org/event/316/contributions/28133/)
[70] Tidikas A. *et al* 2023 Dose rate estimation in IFMIF-DONES lithium loop heat exchanger oil with regard to the different beryllium-7 trapping efficiency *Preprint: 2023 IAEA Fusion Energy Conf.* (*London, United Kingdom, 16–21 October 2023*) TEC/P8–4 (available at: https://conferences.iaea.org/event/316/contributions/28681/)
[71] Kasugai A. *et al* 2023 Progress of engineering design activities for fusion neutron source A-FNS *Preprint: 2023 IAEA Fusion Energy Conf.* (*London, United Kingdom, 16–21 October 2023*) TEC/P1–9 (available at: https://conferences.iaea.org/event/316/contributions/27954/)
[72] Yang Q. *et al* 2023 Development and application of HINEG series high intensity steady neutron generators *Preprint: 2023 IAEA Fusion Energy Conf.* (*London, United Kingdom, 16–21 October 2023*) TEC/P5–10 (available at: https://conferences.iaea.org/event/316/contributions/27959/)
[73] Kargaryan A. *et al* 2023 Upgraded IR-IECF device as a promising compact source for the future nuclear fusion research *Preprint: 2023 IAEA Fusion Energy Conf.* (*London, United Kingdom, 16–21 October 2023*) TEC/P5–2 (available at: https://conferences.iaea.org/event/316/contributions/28835/)
[74] Packer L.W. *et al* 2024 ITER materials irradiation within the D-T neutron environment at JET: post-irradiation radioactivity analysis following the DTE2 experimental campaign *Nucl. Fusion* **64** 106059
[75] Loughlin M.J. *et al* 2023 Recent developments in radiation transport for fusion reactors and validation of JET DT Experiments *Preprint: 2023 IAEA Fusion Energy Conf.* (*London, United Kingdom, 16–21 October 2023*) TEC/P1–3 (available at: https://conferences.iaea.org/event/316/contributions/27951/)
[76] Hill C. *et al* 2023 Fundamental data activities at the IAEA in support of fusion *Preprint: 2023 IAEA Fusion Energy Conf.* (*London, United Kingdom, 16–21 October 2023*) post deadline paper TEC-FNT (available at: https://conferences.iaea.org/event/316/contributions/29351/)
[77] Bailey G.W. *et al* 2023 Latest insights from EU-DEMO activation assessments *Preprint: 2023 IAEA Fusion Energy Conf.* (*London, United Kingdom, 16–21 October 2023*) TEC/P3–7 (available at: https://conferences.iaea.org/event/316/contributions/28138/)
[78] Wu B. *et al* 2023 Development and application of TopMC in fusion shielding *Preprint: 2023 IAEA Fusion Energy Conf.* (*London, United Kingdom, 16–21 October 2023*) TEC/P5–11 (available at: https://conferences.iaea.org/event/316/contributions/28458/)
[79] Young G.J. *et al* 2023 Experimental evaluation of unstructured grid neutron diffusion code *Preprint: 2023 IAEA Fusion Energy Conf.* (*London, United Kingdom, 16–21 October 2023*) TEC/P1–4 (available at: https://conferences.iaea.org/event/316/contributions/27953/)
[80] Tomarchio V. *et al* 2023 Development of preventive and active protection systems for Paschen discharge mitigation for

JT-60SA *Preprint: 2023 IAEA Fusion Energy Conf.* (*London, United Kingdom, 16–21 October 2023*) TEC/P3–8 (available at: https://conferences.iaea.org/event/316/contributions/28132/)
[81] Houry M. *et al* 2023 Protection of the plasma facing components in the west tokamak, progress and development in view of ITER *Preprint: 2023 IAEA Fusion Energy Conf.* (*London, United Kingdom, 16–21 October 2023*) TEC/P5–6
[82] Lampasi A. *et al* 2023 Design novelties in DTT power supply and electrical systems *Preprint: 2023 IAEA Fusion Energy Conf.* (*London, United Kingdom, 16–21 October 2023*) TEC/P8–5 (available at: https://conferences.iaea.org/event/316/contributions/28677/)
[83] Oyarzabal E. *et al* 2023 Overview of the OLMAT high heat flux facility activities testing liquid and solid metal targets for their use as divertor materials *Preprint: 2023 IAEA Fusion Energy Conf.* (*London, United Kingdom, 16–21 October 2023*) TEC/P3–9 (available at: https://conferences.iaea.org/event/316/contributions/28135/)
[84] Tulenbergenov T.R. *et al* 2023 Development of a combined diagnostics system in studies plasma parameters in the radial direction *Preprint: 2023 IAEA Fusion Energy Conf.* (*London, United Kingdom, 16–21 October 2023*) TEC/P1–1 (available at: https://conferences.iaea.org/event/316/contributions/27958/)
[85] Rapp J. *et al* 2023 Towards a MPEX digital twin *Preprint: 2023 IAEA Fusion Energy Conf.* (*London, United Kingdom, 16–21 October 2023*) TEC/P1–5 (available at: https://conferences.iaea.org/event/316/contributions/27959/)
[86] Raj P. *et al* 2023 R&D for the development of compact HHTS coils *Preprint: 2023 IAEA Fusion Energy Conf.* (*London, United Kingdom, 16–21 October 2023*) TEC/P5–9 (available at: https://conferences.iaea.org/event/316/contributions/28456/)
[87] Li P.Y. *et al* 2023 Progress of HTS conductor for compact fusion reactor at SWIP *Preprint: 2023 IAEA Fusion Energy Conf.* (*London, United Kingdom, 16–21 October 2023*) TEC/P8–1 (available at:https://conferences.iaea.org/event/316/contributions/28679/)
[88] Rastogi N. *et al* 2023 AABHAS: a 3 sided fully immersive virtual reality cave facility for design operations & maintenance of nuclear machines *Preprint: 2023 IAEA Fusion Energy Conf.* (*London, United Kingdom, 16–21 October 2023*) TEC/P5–3 (available at: https://conferences.iaea.org/event/316/contributions/28460/)